

Correlation of neural response properties with auditory thalamus subdivisions in the awake marmoset

Edward L. Bartlett^{1,2} and Xiaoqin Wang¹

¹Laboratory of Auditory Neurophysiology, Department of Biomedical Engineering, Johns Hopkins University, Baltimore, Maryland; and ²Central Auditory Processing Laboratory, Departments of Biological Sciences and Biomedical Engineering, Purdue University, West Lafayette, Indiana

Submitted 8 March 2010; accepted in final form 14 March 2011

Bartlett EL, Wang X. Correlation of neural response properties with auditory thalamus subdivisions in the awake marmoset. *J Neurophysiol* 105: 2647–2667, 2011. First published March 16, 2011; doi:10.1152/jn.00238.2010.—As the information bottleneck of nearly all auditory input that reaches the cortex, the auditory thalamus serves as the basis for establishing auditory cortical processing streams. The functional organization of the primary and nonprimary subdivisions of the auditory thalamus is not well characterized, particularly in awake primates. We have recorded from neurons in the auditory thalamus of awake marmoset monkeys and tested their responses to tones, bandpass noise, and temporally modulated stimuli. We analyzed the spectral and temporal response properties of recorded neurons and correlated those properties with their locations in the auditory thalamus, thereby forming the basis for parallel output channels. Three medial geniculate body (MGB) subdivisions were identified and studied physiologically and anatomically, although other medial subdivisions were also identified anatomically. Neurons in the ventral subdivision (MGV) were sharply tuned for frequency, preferred narrowband stimuli, and were able to synchronize to rapid temporal modulations. Anterodorsal subdivision (MGAD) neurons appeared well suited for temporal processing, responding similarly to tone or noise stimuli but able to synchronize to the highest modulation frequencies and with the highest temporal precision among MGB subdivisions. Posterior dorsal subdivision (MGPD) neurons differed substantially from the other two subdivisions, with many neurons preferring broadband stimuli and signaling changes in modulation frequency with nonsynchronized changes in firing rate. Most neurons in all subdivisions responded to increases in tone sound level with nonmonotonic changes in firing rate. MGV and MGAD neurons exhibited responses consistent with provision of thalamocortical input to core regions, whereas MGPD neurons were consistent with provision of input to belt regions.

core; parvalbumin; tone; noise; amplitude modulation

AUDITORY THALAMIC REPRESENTATIONS of sound features form the basis for subsequent cortical computations. The response properties of auditory cortex neurons have been studied in both awake and anesthetized preparations in a number of mammalian species, including primates (Aitkin et al. 1986, 1988; Bartlett and Wang 2005; Bendor and Wang 2008; Brugge and Merzenich 1973; Kajikawa et al. 2005; Wang 2007). Much less is known about the response properties of their inputs from the auditory thalamus, or medial geniculate body (MGB), particularly in awake animals (Jones 2003; Hu 2003; Winer et al. 2005). Without adequate knowledge of response properties of

the MGB subdivisions, it is difficult to determine the extent to which the response properties of auditory cortex neurons have been inherited from MGB inputs or result from thalamocortical and/or intracortical processing.

In primates, the MGB has been subdivided on the basis of cytoarchitecture, myeloarchitecture, cytochrome oxidase activity, and immunoreactivity for the calcium binding proteins calbindin and parvalbumin (de la Mothe et al. 2006; Hashikawa et al. 1991; Jones 2003; Jones et al. 1995; Molinari et al. 1995). Similar patterns of parvalbumin and calbindin distribution have been described for other species (Cruikshank et al. 2001; de Venecia et al. 1995; Rubio-Garrido et al. 2007). The ventral division (MGV) is part of the auditory core pathway that projects to the input layers of primary auditory cortex. It stains strongly for parvalbumin and weakly for calbindin (Hackett et al. 1998; Jones 2003). The posterodorsal division (MGPD) produces a complementary pattern of staining, weaker for parvalbumin and stronger for calbindin. MGPD projects to nonprimary auditory cortex and appears to be analogous to the dorsal division (MD) and caudodorsal division described in other species (Calford and Aitkin 1983; de la Mothe et al. 2006; Hackett et al. 1998; Winer 1984, 1992). In primates, there is also an anterodorsal division (MGAD), characterized by moderate staining for both parvalbumin and calbindin and by its projections to primary and nonprimary auditory cortex (Jones 2003; Jones et al. 1995; Molinari et al. 1995). Finally, the medial division (MGM) and suprageniculate (SG) have widespread projections to auditory cortex and receive auditory and nonauditory inputs in cats, rodents, and primates (Hackett et al. 1998; Winer 1984, 1992).

Whereas studies of MGB response properties in primates have focused on either spectral (Allon et al. 1981; Kajikawa et al. 2005) or temporal properties (Preuss and Muller-Preuss 1990), no primate study has attempted to correlate both of those categories of properties with location within the MGB. Previous studies have largely focused on MGV. Much less is known about the response properties of MGD neurons, particularly in awake animals. Studies in cats (Calford 1983; Calford and Aitkin 1983), rats (Bordi and Ledoux 1994), and guinea pigs (Anderson et al. 2007; Edeline et al. 1999) focused on spectral tuning properties and demonstrated MGD responses to tones with long latencies and broad or labile tuning.

In addition to differences between subdivisions, studies by Rouiller and colleagues (Rodrigues-Dagaeff et al. 1989; Rouiller et al. 1989, 1990) found physiological and anatomical response differences between rostral and caudal MGB, such as an increase in GABAergic neurons going from rostral to caudal in MGV

Address for reprint requests and other correspondence: E. L. Bartlett, Depts. of Biological Sciences and Biomedical Engineering, Purdue Univ., 206 S. Martin Jischke Dr., MJIS 2023, West Lafayette, IN 47907 (e-mail: ebartle@purdue.edu).

and an increase in nonmonotonic responses (Rouiller et al. 1990). Such physiological differences may be correlated with different thalamocortical projections to auditory cortex (Read et al. 2010; Storace et al. 2010) and with inputs from inferior colliculus (IC) (Rodriguez et al. 2010).

We have studied the responses of MGB neurons in awake marmosets. In the present study, we compared the responses to temporally modulated stimuli and stimuli with varying degrees of spectral complexity across different MGB subdivisions. The subdivisions were identified anatomically by their cytoarchitecture, myeloarchitecture, and differential immunoreactivity for parvalbumin and calbindin. Some response properties, such as nonmonotonicity of the rate-level function, were found throughout the MGB. In addition, neurons in each subdivision were found to form separable response populations that are likely to reflect a functional segregation. Our results suggest that multiple, parallel functional pathways can be identified anatomically and physiologically in the auditory thalamus and form the basis for functionally segregated pathways in auditory cortex. They further suggest that MGB regions with similar spectral response properties may differ substantially in temporal response properties.

METHODS

Animal Preparation and Single-Unit Recording Procedures

All experiments were performed at Johns Hopkins University in AAALAC-approved facilities following protocols approved by the Institutional Animal Care and Use Committee. The methods for preparing marmoset monkeys for chronic electrophysiological recording have been previously reported (Lu et al. 2001). Some modifications were made for recording from MGB neurons (Bartlett and Wang 2007) and are briefly described. The recording electrode (3–5 MΩ, tungsten electrode; A-M Systems) approached the MGB in a dorsolateral-to-ventromedial trajectory. The electrode entered ~3 mm lateral to the high-frequency representation of A1 along the lateral sulcus at an angle of 57.5°. The tracks can be recreated or adapted for future experiments using the freely available StereoNavi 3.0 software in conjunction with an online marmoset atlas (Tokuno et al. 2009). Auditory responsive neurons were encountered ~6–9 mm after the cortical surface was penetrated (usually 6.5–7.0 mm). The rostral half of the MGB is bordered laterally by the lateral geniculate nucleus. Therefore, it was possible to determine that the MGB was nearby when one passed through a region of visually responsive neurons followed by 200–700 μm without encountering any spiking neurons.

Acoustic Stimuli

Stimuli were presented in free-field from a speaker (B&W 601) located 70 cm in front of the animal and level with the animal's head (0° azimuth, 0° elevation). The interiors of the double-walled sound-proof chambers (Industrial Acoustics) in which recordings took place were covered with 3-in. acoustic absorption foam (Sonex, Ilbruck, MN). Stimuli were created from custom programs using MATLAB software (The Mathworks, Natick, MA), generated through a digital-to-analog converter (Tucker-Davis Technologies, Alachua, FL) with a 100-kHz sampling rate, low-pass filtered at 50 kHz, attenuated with two serially linked attenuators (Tucker-Davis Technologies), and amplified by a power amplifier (Crown International, Elkhart, IN). The measured speaker output was calibrated to ±4 dB for frequencies from 100 Hz to 36 kHz, which encompasses the hearing range of marmosets, with a calibrated sound level of 90 dB SPL at 0-dB attenuation for 1-kHz tones.

Tone frequency tuning. When a neuron was isolated, its preference for tones was assessed initially using a manually controlled oscillator and attenuators to obtain an estimate of the neuron's best frequency (BF) and best sound level. Following this procedure, tone frequency tuning was tested by presenting tones (minimum 10 tones/octave) at the estimated best level over a three- to four-octave range centered on the estimated BF. Tone stimuli were 200 ms in duration. If no frequency generated clear responses during hand tuning, tones were tested with tone frequencies from 0.5 to 32.0 kHz (10 tones/octave), usually at 60 dB SPL or 60 dB and also 20–30 dB SPL. We found that many neurons in the MGB were difficult to drive if we did not sample densely enough or were inhibited if the sound level was too high.

The tone frequency that produced the highest consistent firing rates, which was the neuron's BF, was then used to test the neuron's sound level preference. Sound level was typically changed from –10 to 80 dB SPL in 10-dB steps to obtain a rate-level function for the neuron and determine the neuron's best level. Finally, many units were tested for tone frequency tuning again. This time, tone frequencies were densely sampled (usually 20 tones/octave) over a one-octave range centered at the neuron's BF and at the neuron's best level. Again, the dense sampling of stimulus frequencies sometimes revealed response properties that could have been overlooked if frequencies had been sampled sparsely, such as the presence of a second frequency peak or lateral inhibition.

Band-pass noise stimuli. For neurons with demonstrated BFs derived from responses to tone stimuli, band-pass noise (BPN) stimuli were centered at the neuron's BF and presented at the neuron's best level. Noise bandwidth was then varied from 0.1 to 2.1 octaves in 0.2-octave steps. BPN stimuli were 200 ms in duration.

For neurons that were not clearly responsive to tones, BPN stimuli with center frequencies of 0.5–32.0 kHz were presented with 0.5 or 1.0 octaves of bandwidth. Center frequency spacing was 5–8 center frequencies/octave. Once a best center frequency was obtained, noise bandwidth was varied from 0.1 to 2.1 octaves in 0.2-octave steps.

Click train stimuli. The sound stimuli used were either 0.1-ms rectangular clicks or Gaussian clicks. Gaussian clicks are tones whose amplitude envelope is a Gaussian whose duration and bandwidth can be controlled by controlling the variance of the Gaussian, which is the parameter termed sigma. Details of the click stimuli have been discussed in Lu et al. (2001) and Bartlett and Wang (2007). For each neuron reported in the current study, neurons were tested with click trains of 500–1,000 ms in duration with a set of interclick intervals (ICIs) that varied from 1 to 100 or 1 to 150 ms. Spiking activity was recorded for 500 ms preceding each click train and for at least 500 ms after the offset of the sound stimulus. There was at least 1 s of silence between each stimulus. Each click train stimulus was repeated 5–10 times.

Sinusoidally amplitude-modulated stimuli. Sinusoidally amplitude-modulated tone (SAM) or sinusoidally amplitude-modulated noise (NAM) stimuli used the neuron's BF as the carrier frequency. For NAM stimuli, the neuron's best center frequency and best bandwidth were used as the carrier. SAM and NAM stimuli were 500 or 750 ms in duration. Modulation frequency was varied from 4 to 1,024 Hz in one-octave or, occasionally, one-half-octave steps. The bandwidths of the NAM stimuli were almost always greater than the maximum modulation frequency, so frequency sidebands generated by amplitude modulation were within the noise band.

Data Analysis

Spontaneous rate was computed as the mean rate of the periods (200 or 500 ms) that preceded each trial. Driven firing rate was computed as the overall firing rate during the presentation of the stimulus minus the spontaneous rate.

Tone frequency tuning. BF was defined as the tone frequency that generated the highest firing rate in the recorded neuron. The 50% response bandwidth, or halfwidth, was defined as the bandwidth at

which the firing rate was $\leq 50\%$ of the peak firing rate on both sides of the peak. The points at which the firing rate crossed the 50% response rate were obtained by linearly interpolating between responses to two consecutive frequency steps that were above and below 50%, respectively. Firing rate suppression was defined as the frequency nearest to BF at which the driven rate was below zero (i.e., below spontaneous rate). Firing rate suppression was measured separately for frequencies below BF and those above BF. Multipeaked responses were defined for frequency tuning curves for which the firing rate at off-BF frequencies was significantly elevated ($P < 0.05$ vs. spontaneous rate, rank-sum test) and was $> 50\%$ of the firing rate at BF. These stringent criteria were used to isolate clear multipeaked responses. An additional 20/131 units (16%) tested had responses in which the secondary firing rate was significantly elevated ($P < 0.05$ vs. spontaneous rate, rank-sum test) but was $< 50\%$ of the peak firing rate at BF. In many of these 20 units, the spikes for the weak secondary peak were not obviously time-locked to the stimulus onset.

Tone rate-level. Best level was defined as the sound level that produced the maximum statistically significant firing rate ($P < 0.05$ vs. spontaneous rate, rank-sum test). The monotonicity index of a given unit was defined as the total firing rate (driven rate + spontaneous rate) in response to the loudest sound level (usually 80 dB in the present study) divided by the maximum total firing rate at the best level. A unit was considered “monotonic” if its monotonicity index was > 0.75 , “weakly nonmonotonic” if its monotonicity index was between 0.75 and 0.25, and “strongly nonmonotonic” if its monotonicity index was < 0.25 . The rate-level (RL) halfwidth was defined in the same way as frequency above but using steps in sound level rather than frequency. Only nonmonotonic units were analyzed for RL halfwidth. For monotonic units, the dynamic range was calculated as the difference between the threshold level and the best level. Threshold was calculated as the sound level at which the linearly interpolated firing rate was greater than the spontaneous rate plus two standard deviations of the spontaneous rate. The response latency was the earliest time at which the rate was greater than the spontaneous rate plus 2.5 times the standard deviation of the spontaneous rate.

Band-pass noise. Best bandwidth was defined as the noise bandwidth that produced the highest driven firing rate over the total stimulus duration. A bandwidth bias was calculated by comparing the difference between the maximum firing rates for narrow bandwidths (≤ 0.5 octaves) and broad bandwidths (> 1 octave) divided by their sum. A bandwidth bias greater than 0.2 (narrowband rate at least 50% higher than broadband rate) was considered to be “narrowband preferring,” whereas a bias less than -0.2 was considered “broadband preferring.”

Click train. The ability to synchronize to a click train was quantified by measuring the vector strength of the neuronal response at each ICI. Statistical significance was assessed using the Rayleigh statistic, which also takes into account the number of spikes evoked by the stimulus (Lu et al. 2001). A threshold Rayleigh statistic value of 13.8 was considered significant ($P < 0.001$). Many units produced significant, nonsynchronized increases in firing rate for short ICI stimuli. Synchronized units generated stimulus-synchronized responses for longer ICIs and onset responses for shorter ICIs. Those that only produced nonsynchronized changes in firing rate were defined as nonsynchronized units. Those that generated synchronized responses for longer ICIs and sustained increases in firing rate for shorter ICIs were defined as mixed units, consistent with Bartlett and Wang (2007).

For each unit, the maximum click rate at which the neuron was significantly synchronized was called Fmax, given as $F_{max} = 1/(synchro-$ nization boundary). A rate boundary was computed for neurons that had statistically significant driven firing rates ($P < 0.05$ vs. spontaneous firing rate, rank-sum test) in response to stimuli with ICIs ≤ 5 ms. The rate boundary was the ICI for which the interpolated driven firing rate crossed the threshold of twice the standard deviation

of the spontaneous rate. Click latency was computed the same way as the latency for rate-level responses described above.

Amplitude-modulated sounds. Similar to analysis of click responses, an Fmax was computed. In addition, the rate-best modulation frequency was calculated as the weighted average of the modulation frequencies weighted by their firing rates. Only statistically significant responses whose steps were continuous with the modulation frequency that produced the peak firing rate were used. Because modulation frequencies were stepped in 0.5- to 1-octave steps, modulation frequencies were converted to a log₂ scale before the weighted average was computed.

Anatomy

At the cessation of recording, small electrolytic lesions were made in physiologically identified regions of MGB by passing 8- μ A current through the recording electrode (6–10 s at each polarity). For the animal whose MGB is shown in Fig. 1, from whom the largest number of units were obtained, large lesions were made by passing 1.1 mA through the recording electrode (7 s at each polarity). Animals were euthanized by administering an initial intramuscular injection of ketamine followed by an intraperitoneal injection of Euthasol (100 mg/kg; Virbac, Milperra, Australia).

Animals were transcardially perfused with room temperature PBS with heparinized phosphate buffer (pH ~7.0) followed by 4% paraformaldehyde (EM grade; Ted Pella, Redding, CA) in 0.1 M phosphate buffer (pH ~7.0). After perfusion, the brain was removed, put in 30% sucrose solution, and frozen. Sections (30 μ m) were cut on a freezing microtome through the entire extent of the MGB. Sections were processed for Nissl staining, parvalbumin immunoreactivity, and calbindin immunoreactivity using standard histological procedures (Jones and Hendry 1989). Myelin staining followed a modified Gallyas stain protocol (Pistorio et al. 2006).

MGB subdivisions were assigned based on parcellation schemes established in previous studies of the MGB in macaques (Hashikawa et al. 1995; Jones 2003; Kaas and Hackett 2000; Molinari et al. 1995), owl monkeys (Morel and Kaas 1992), and marmosets (Aitkin et al. 1988; de la Mothe et al. 2006). The locations of recorded neurons in the MGB were reconstructed based on the coordinates of the tracks relative to the tracks in which lesions were made and the depths at which the recordings occurred.

RESULTS

For this study, 320 well-isolated single units were recorded from the MGB of three marmoset monkeys. Of these, 301 units could be localized to one of the three subdivisions described below. The small number of neurons recorded in the MGM and SG ($n = 8$) were not included in analyses, nor were the 11 units that could not be localized to an MGB subdivision.

Anatomical Characterizations of MGB Subdivisions

Marmoset brains were removed, sectioned, and stained for Nissl, myelin, and the calcium-binding proteins parvalbumin and calbindin, which have been shown to differentiate core from belt nuclei, respectively, in the auditory thalamus and cortex of macaques and mice (Cruikshank et al. 2001; Jones 2003). Figure 1 shows sections going from rostral (Fig. 1, A–H) to caudal (Fig. 1, I–P) for one representative animal; the left column of panels shows Nissl staining, the second column shows myelin staining, the third column shows calbindin staining, and the right column shows parvalbumin staining.

MGV. The marmoset MGV (region marked “V” in Fig. 1) is characterized by densely packed small and medium-sized cells in Nissl (Fig. 1A), moderate to strong parvalbumin staining

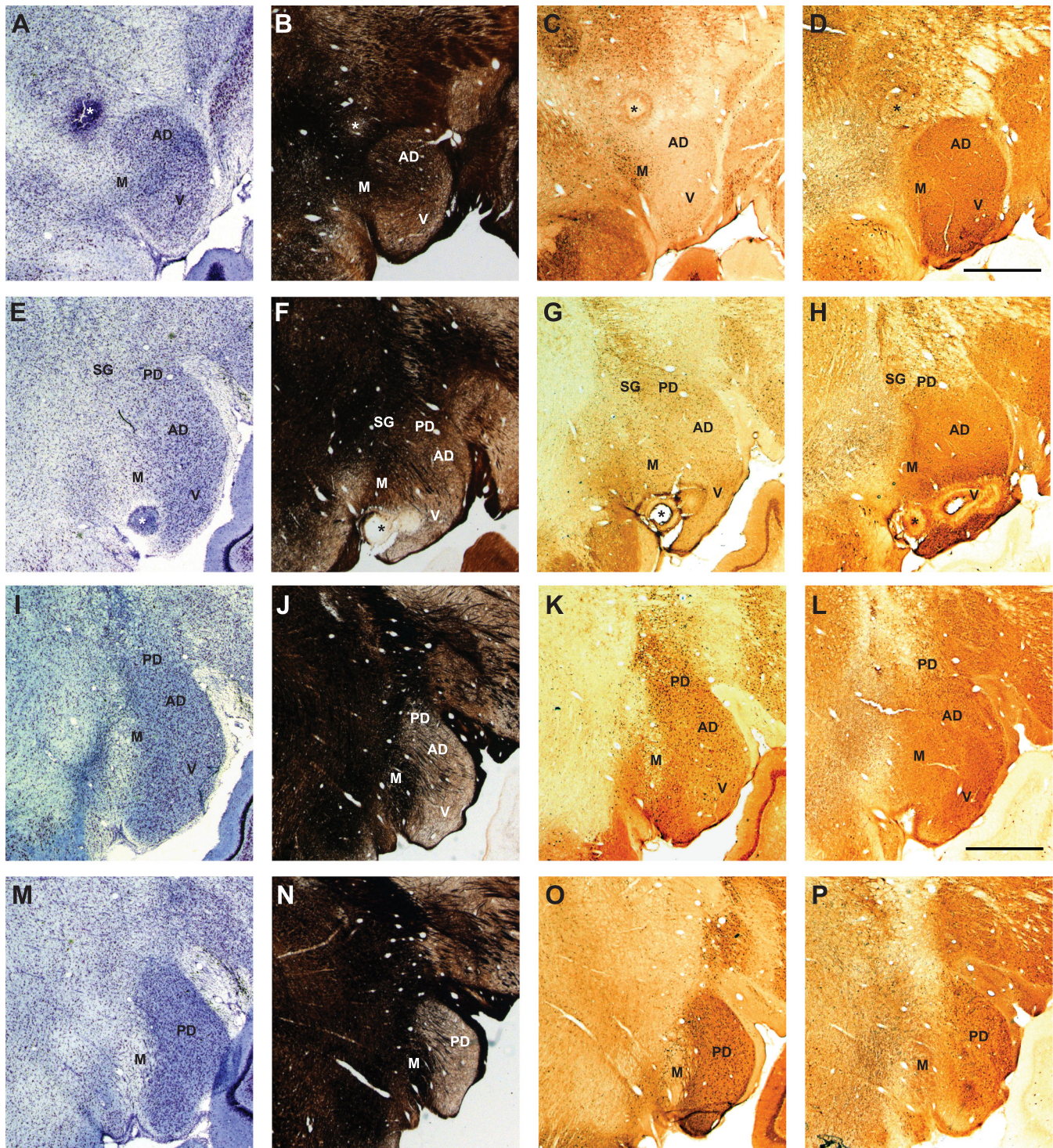


Fig. 1. Comparison of medial geniculate body (MGB) subdivisions using Nissl, myelin, and calcium-binding protein immunolabeling. The MGB is shown in coronal sections going from anterior (*A*) to posterior (*P*) with dorsal toward the top and lateral to the right. *A, E, I, M*: Nissl stain. *B, F, J, N*: myelin stain (modified Gallyas stain; Pistorio et al. 2006). *C, G, K, O*: calbindin immunolabeling. *D, H, L, P*: parvalbumin immunolabeling. MGB subdivisions, including the ventral division (V), anterodorsal division (AD), posterodorsal division (PD), medial division (M), and suprageniculate (SG), are labeled. Asterisks denote locations of electrolytic lesions. The scale bars are 1 mm and apply to all panels.

(Fig. 1*D*), and relatively weak calbindin staining (Fig. 1*C*). The ventral division of MGB (MGV) extends along the rostral 75% or so of the MGB (>1.5 mm). It is present at the rostral pole of the MGB (Fig. 1, *A–D*). The MGV then expands laterally and dorsally and is the main MGB subdivision in the rostral

one-third of MGB (Fig. 1, *A–H*). About midway through the MGB, the MGV begins to decrease in size in its dorsal aspect and disappears in the caudal end of MGB (Fig. 1, *I–P*). Myelin staining showed a medial to lateral gradient in MGV (Fig. 1, *B* and *F*) where myelin staining was weaker than in MGAD

(described below). Parvalbumin staining in MGV included regions of high staining intensity ventrally and laterally in MGV. Parvalbumin-positive cell bodies were densest in a shell extending around the dorsal, lateral, and ventral edges of MGB, including the ventralmost MGV (Fig. 1, *D* and *L*). Calbindin labeling in MGV in fibers and in cell bodies increased from rostral to caudal (Fig. 1, *C*, *G*, *K*, and *O*). A large electrolytic lesion can be seen traversing the MGV in this animal (Fig. 1, *E–H*, asterisks).

MGPD. The posterodorsal division of MGB (region marked “PD” in Fig. 1) appears at the dorsomedial edge of MGB about midway through the rostrocaudal extent. Going caudally, it expands ventrally and laterally, forming the caudal edge of the MGB (Fig. 1, *D–F*). MGPD neurons are moderately or loosely packed with a variety of sizes, mostly small and medium sized (Fig. 1, *I* and *M*). Parvalbumin labeling was weaker in MGPD than in MGV and was concentrated in the lateral aspect of MGPD (Fig. 1*P*). There was some variability in the degree of parvalbumin labeling, with very little labeling in the caudal MGB of one animal, especially near the caudal pole. Calbindin labeling of fibers and cell bodies was relatively high in MGPD (Fig. 1, *K* and *O*), and cell body labeling was denser than in MGAD or MGV. Myelin-labeled fibers (Fig. 1, *J* and *N*) can be seen entering MGPD and radiating laterally and ventrally. Myelinated fibers appear to have entered more dorsally in caudal MGB compared with the rostral two-thirds of MGB.

MGAD. The anterodorsal division of MGB (region marked “AD” in Fig. 1) appears dorsally in the MGB near the rostral pole and expands going caudally (Fig. 1, *A–H*). In the caudal half of MGB, MGAD decreases in size and is replaced by MGPD dorsally (Fig. 1, *I–P*). It can be distinguished from MGV by its higher proportion of larger cells (Fig. 1, *A* and *E*) and greater presence of myelinated fibers (Fig. 1, *B* and *F*). The change in Nissl pattern corresponding to MGAD generally occurred at or slightly dorsal to the main extension of myelinated fibers, most likely from IC axons, from the medial aspect of MGB. There was a rostrocaudal gradient of calbindin labeling in MGAD, with more calbindin labeling caudally (cf. Fig. 1, *C* and *K*). A second electrolytic lesion can be seen medial to MGAD in the most rostral section (Fig. 1, *A–D*, asterisks).

MGM. The medial division of MGB (region marked “M” in Fig. 1) forms a thin slab along the medial edge of the MGB that runs from the caudal MGB almost to the rostral pole of MGB (Fig. 1, *B–F*). It has the lowest cell density of any of the MGB subdivisions. Myelin staining was quite strong in MGM (Fig. 1, *B*, *F*, *J*, and *N*). The transition from very dense myelin staining to ramifying myelinated fibers marks a transition from MGM to the more lateral MGB subdivisions, especially in the ventral half of MGB. MGM stained weakly to moderately for parvalbumin (Fig. 1, *D*, *H*, *L*, and *P*) and moderately to strongly for calbindin (Fig. 1, *C*, *G*, *K*, and *O*). Parvalbumin-positive fibers can also be seen medial to MGM, which are axons from the brachium of the IC (Fig. 1, *D*, *H*, *L*, and *P*). In addition, parvalbumin-positive cells can be seen scattered in MGM, especially in Fig. 1, *D* and *L*. By contrast, the hippocampus adjacent to MGB is almost devoid of parvalbumin staining.

SG. The suprageniculate nucleus is a smaller group of cells that extends dorsally and medially away from the dorsomedial corner of MGM, MGAD, and MGPD. It is found in the middle

half of MGB rostrocaudally (Fig. 1, *E–H*). It stained more densely for myelin than MGPD (Fig. 1*F*) and is often separated from the main portion of MGB by a thin region of loosely packed cells.

Because our electrodes approached the MGB laterally, we rarely recorded from what we believe were MGM and SG ($n = 8$ units combined from all 3 animals). Therefore, we have not included these subdivisions in our descriptions of MGB response properties.

Physiological Properties of MGB Subdivisions: Responses to Pure Tones

For each animal, unit locations were determined based on their locations relative to electrolytic lesions and the relative locations of the electrode tracks. Unless stated, the reported neurons only include neurons found in MGV, MGAD, and MGPD.

Spontaneous firing rate. Almost all MGB units were spontaneously active. To compare between subdivisions, the spontaneous firing rates for each unit tested for frequency tuning or for rate-level were averaged for each subdivision. In MGV, MGAD, and MGPD, spontaneous firing rates were similar (Fig. 2*A*; $P > 0.05$, Kruskal-Wallis test). Most neurons in these subdivisions discharged at 3–10 spikes/s in the absence of sound stimulation while the animal was awake (Fig. 2*A* and Table 1), with a median rate of 7.2 spikes/s ($n = 193$).

Distribution of best frequency. Frequency tuning to pure tones was assessed in 173 single units recorded from 3 animals. Statistically significant excitatory responses were observed in 134 units. The 39 other units were not driven or were only inhibited by tones at the sound levels at which they were tested. Figure 2*C* shows the distribution of recorded BFs and thresholds superimposed on the marmoset audiogram of Seiden (1957). BF of the units ranged from 0.5 to 32.5 kHz (Fig. 2*B*), with a preponderance of responses in the 4- to 16-kHz range. The most sensitive responses were found in this range, as expected from the behavioral audiogram (Seiden 1957). BF was not distributed evenly in all MGB subdivisions. The BFs of MGAD neurons were significantly lower than those of all the other subdivisions (Fig. 2, *B* and *C*, and Table 1). The BFs of two-thirds (18/27) of MGAD neurons were tuned to frequencies <4.0 kHz, whereas much smaller proportions of MGV and MGPD neurons (7/25) were tuned to that frequency range ($P < 0.05$, MGAD vs. MGV, MGPD, χ^2 test).

Tone frequency tuning. Figure 3 illustrates the types of frequency tuning commonly observed in the MGB of awake marmosets. Frequency tuning was often quite narrow (Fig. 3, *A*, *B*, and *D*) with evidence of lateral inhibition shaping the tuning width of neuronal responses. For these neurons, sparse sampling along the frequency axis would likely miss the neuron’s excitatory responses or lateral inhibition. Figure 3*A* shows an example of a narrowly tuned MGV neuron. Frequency was varied from 4 to 16 kHz in 24 steps, but only 11.3-kHz tones were able to generate a significant response. The halfwidth of this neuron was less than one semitone (1/12th octave), which is substantially narrower than reported auditory nerve (Evans 1972; Pickles 1979) or IC inputs (Ramachandran et al. 1999; Ryan and Miller 1978), but it was not extraordinary in our sample. Lateral inhibition, defined in our study as a sound-evoked decrease in firing rate below the

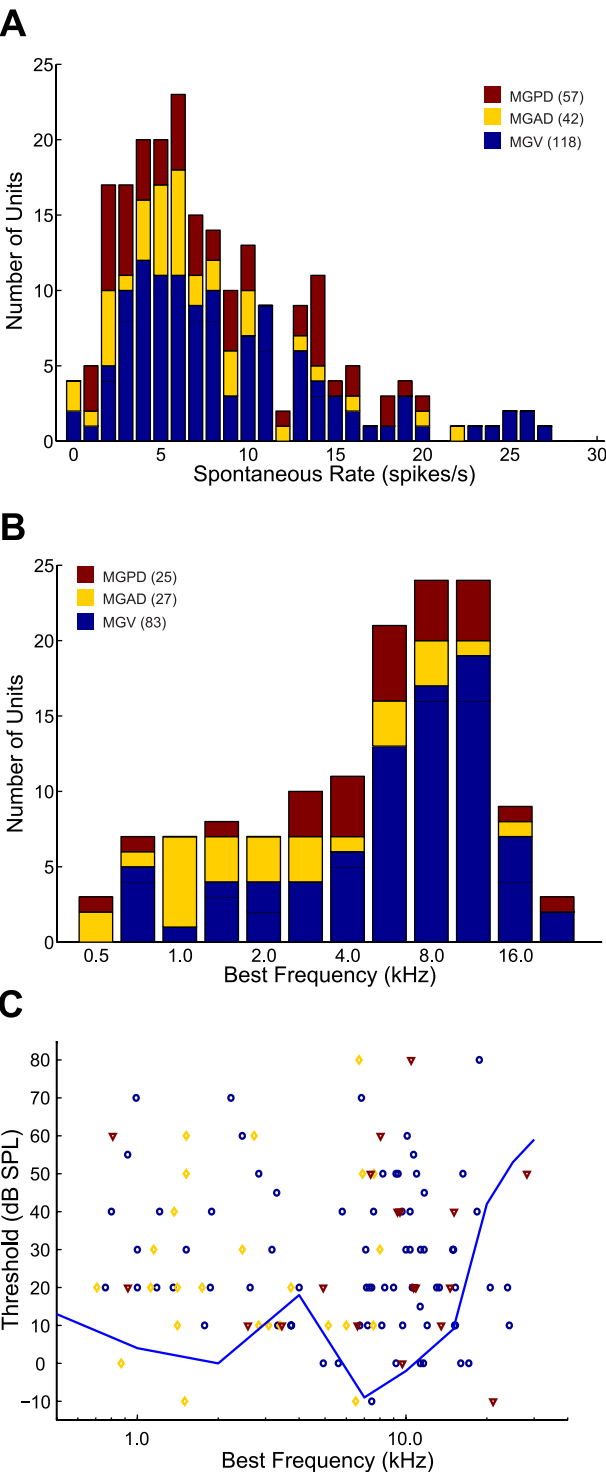


Fig. 2. Population best frequency (BF) and spontaneous rate distributions. *A*: histogram of spontaneous firing rates for each MGB subdivision: ventral (MGV; blue), anterodorsal (MGAD; yellow), and posterodorsal (MGPD; red). The number of units n is given in parentheses for each subdivision. *B*: histogram of BF for each MGB subdivision. *C*: threshold plotted as a function of BF for neurons in MGV, MGAD, and MGPD. The blue line shows a behavioral audiogram of the marmoset with values taken from Seiden (1957).

spontaneous rate that is within 0.25 octaves of BF, was evident on both the high- and low-frequency sides of the peak (Fig. 3*B*). Broadly tuned neurons (Fig. 3*C*) and neurons that were inhibited by tone stimuli (not shown) were less commonly

observed than neurons with narrowly tuned excitation. Given prior suggestions that cells in dorsal MGB are broad bandwidth (Bordi and Ledoux 1994; Calford 1983), a surprising observation was that about one-half of the MGPD neurons that were responsive to tones were sharply tuned (Fig. 3*E*). An example of a sharply tuned MGPD neuron is shown in Fig. 3*D*.

Overall, the tone tuning halfwidths were uniformly narrow, even in MGPD. Figure 3*E* compares the halfwidths across subdivisions. They were narrowest in the MGV and significantly broader in MGPD with similar trends in MGAD that did not reach statistical significance (Table 1). The narrow tuning was not simply the result of examining frequency tuning at a single sound level. Figure 3*G* compares the tuning for 38 units whose frequency tuning was tested at best level and a softer sound level (-19 dB on average). Figure 3*H* compares the tuning for 39 units whose frequency tuning was tested at best level and a louder sound level ($+20$ dB on average). In both cases, tuning was quite narrow at best level and at the other sound level tested. Moreover, due to the nonmonotonic nature of most rate-level responses (discussed below), the firing rates were much lower away from best level. Such level-tolerant tuning has been observed in both the IC inputs to the marmoset MGB (Nelson et al. 2009) and in the marmoset auditory cortex (Sadagopan and Wang 2008).

The observed narrow frequency tuning was likely due to inhibition that sharpened the frequency response. To determine the nearest frequencies at which inhibition balanced or exceeded excitation, we measured the frequencies relative to the BF at which the driven rate fell below zero, meaning below the spontaneous rate (Table 1, near negative low and near negative high, and Fig. 3*F*). In the MGV, inhibition on both the high- and low-frequency sides of the frequency tuning curve was prevalent. This can be seen on the high- and low-frequency sides of the frequency tuning curves in the examples in Fig. 3, *A–D*. For MGV neurons, the median frequency difference at which the driven rate was driven below the spontaneous rate was only 0.14 octaves on the high-frequency side and 0.16 octaves on the low-frequency side. In the other subdivisions, inhibition was not as prevalent or not observed as close to BF as in MGV. On the high-frequency side, inhibition was observed significantly farther from BF in MGAD and MGPD neurons compared with MGV neurons (Fig. 3*F* and Table 1).

Table 1. Frequency tuning properties by MGB subdivision

	MGV	MGAD	MGPD
Spontaneous rate, spikes/s	9.6 ± 7.2 (118)	6.8 ± 4.9 (42)	8.0 ± 5.4 (57)
BF, kHz	9.0 ± 5.9 (87)	4.2 ± 4.1^a (27)	8.6 ± 6.5 (24)
Halfwidth, octave	0.16 ± 0.13^b (87)	0.20 ± 0.17 (27)	0.21 ± 0.14 (24)
$Q_{\text{Best level}}$, dB	13.2 ± 7.2^b (87)	12.1 ± 6.8 (27)	9.9 ± 6.3 (24)
Near negative low	-0.25 ± 0.22 (65)	-0.32 ± 0.26 (21)	-0.30 ± 0.24 (18)
Near negative high	0.21 ± 0.16^c (70)	0.38 ± 0.33 (26)	0.28 ± 0.25 (17)
Single peaked, %	86 (73)	56 (27)	58 (24)
Inhibited, %	62 (73)	22 (27)	38 (24)

Values are means \pm SD; numbers in parentheses indicate number of units for each medial geniculate body (MGB) subdivision: ventral (MGV), anterodorsal (MGAD), and posterodorsal (MGPD). BF, best frequency; $Q_{\text{Best level}}$, Q value measured at the unit's best sound level as assessed by firing rate; Near negative low and near negative high, the nearest frequencies at which the driven response (rate – spontaneous rate) is ≤ 0 spikes/s. ^a $P < 0.01$ vs. MGV and MGPD (Kruskal-Wallis test). ^b $P < 0.05$ vs. MGPD, Kruskal-Wallis test. ^c $P < 0.01$ vs. MGAD and MGPD, Kruskal-Wallis test.

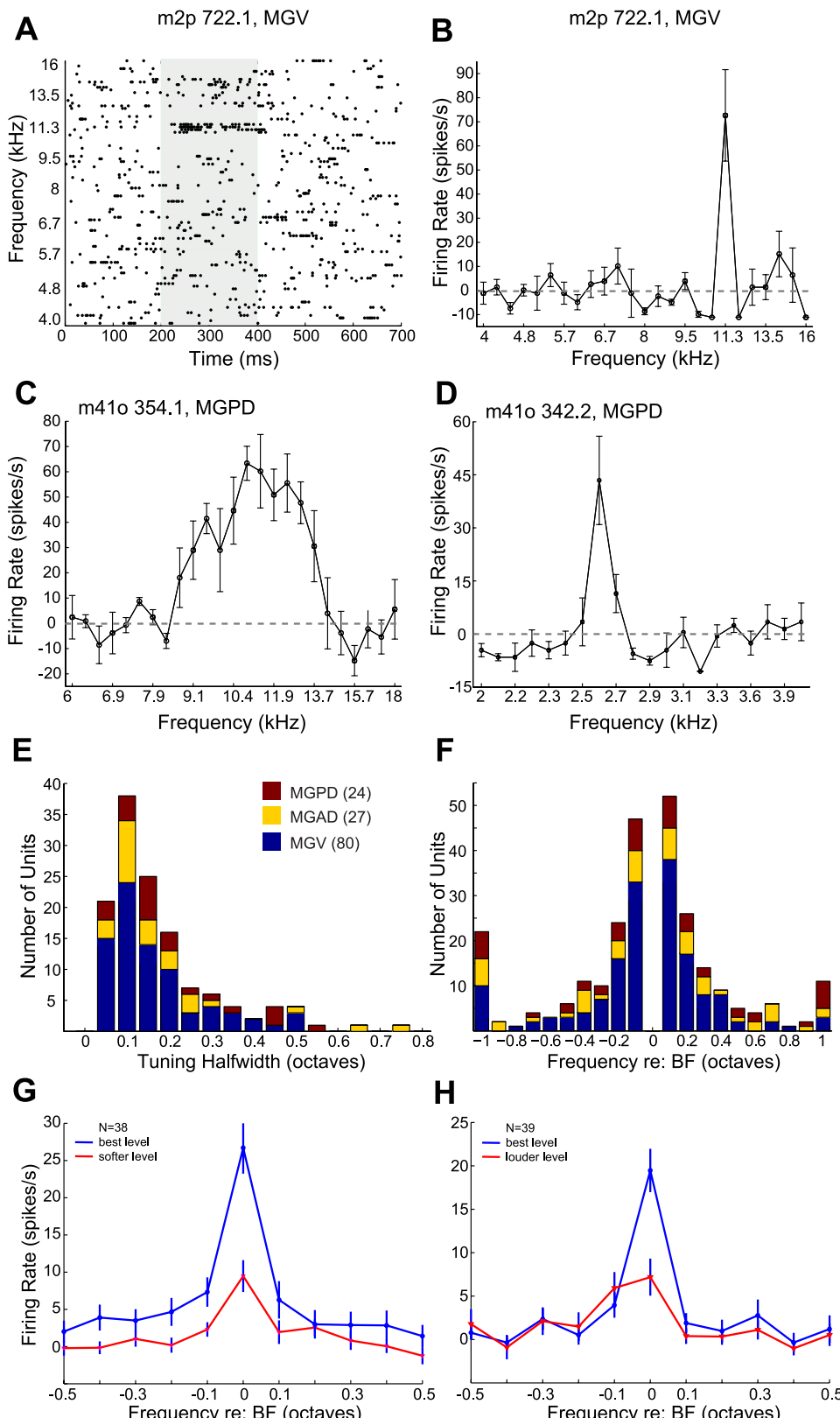


Fig. 3. Tone frequency tuning is sharp and shaped by inhibition in MGB units. *A*: dot raster plot of responses of MGV unit m2p-722.1 to tones of different frequencies. Frequency = 4.0–16.0 kHz, 25 frequencies. In all examples, frequency steps are logarithmically spaced. Sound level = 20 dB. All sound level values are dB SPL. Each dot represents 1 action potential. The shaded region indicates the onset and duration of the stimulus. *B*: driven firing rate as a function of tone frequency for MGV unit m2p-722.1. In all examples, the spontaneous rate has already been subtracted so that inhibition may be more easily observed. Values are means \pm SE. Dashed line indicates zero driven firing rate (i.e., firing rate = spontaneous rate). Unless stated otherwise, firing rate was averaged over the stimulus duration. *C*: driven firing rate as a function of tone frequency for MGPD unit m41o-354.1. Frequency = 6.0–18.0 kHz, 25 frequencies. Sound level = 50 dB. *D*: driven firing rate as a function of tone frequency for MGPD unit m41o-342.2. Frequency = 2.0–4.0 kHz, 20 frequencies. Sound level = 20 dB. *E*: histogram of 50% response bandwidth of tone tuning curves for different MGB subdivisions. Estimates of tuning were based on a minimum of 10 steps/octave. *F*: negative firing rates often occur close to BF in all subdivisions. Histogram shows observations of a negative firing rate (i.e., driven rate < spontaneous rate) as a function of the frequency difference from BF. Histograms were computed separately for frequencies above BF (positive values) and below BF (negative value). If a unit had not decreased its firing rate below spontaneous within ± 1 octave, it was assigned a value of ± 1 . *G*: frequency tuning at best level (blue line) and tested at a level below best level (red line; -19 dB on average) for 38 MGB units. *H*: frequency tuning at best level (blue line) and tested at a level above best level (red line; +20 dB on average) for 39 MGB units.

Multipeaked responses. Multipeaked frequency tuning has previously been observed in auditory cortex of awake marmosets (Kadia and Wang 2003). Of the 134/173 units that had a clearly defined excitatory BF, 32 units had multipeaked responses in which the firing rate at off-BFs was significantly elevated (see

METHODS). One example of a multipeaked response is shown in Fig. 4, *A* and *B*. In this MGAD neuron, the BF was 8.0 kHz and the secondary peak occurred at 6.7 kHz (0.26-octave difference). The BF peak and the secondary peak were distinct because a 7.7-kHz tone significantly inhibited the unit (Fig. 4*A*).

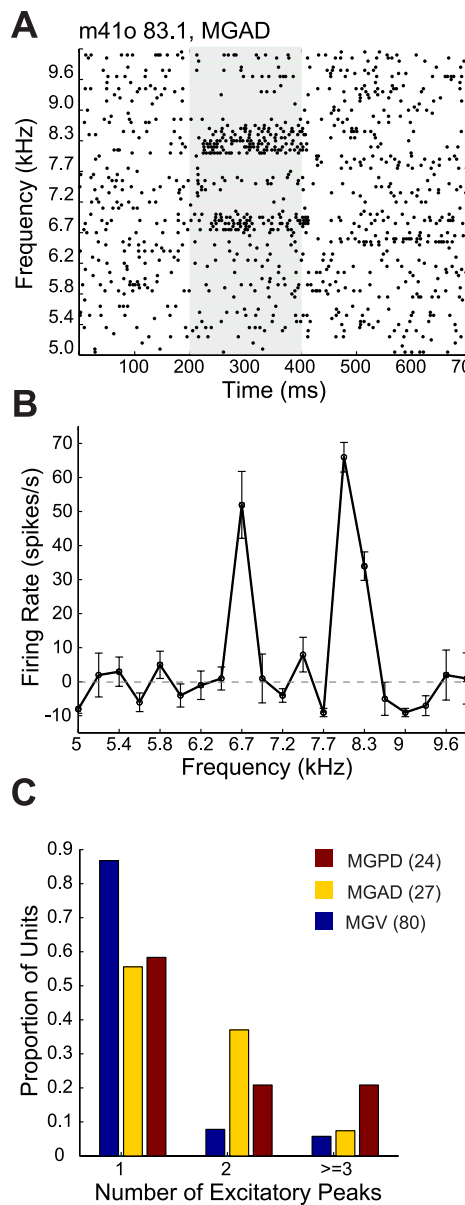


Fig. 4. Neurons in the MGV are typically single peaked, whereas those in MGAD and MGPD are often multipeaked. *A*: dot raster plot of an example of a multipeaked neuron (MGAD unit M41o-83.1). Frequency = 5.0–10.0 kHz, 20 frequencies. Sound level = 30 dB. *B*: driven rate as a function of tone frequency, showing 2 distinct peaks at 6.7 and 8.0 kHz. Units were considered multipeaked if 2 or more excitatory peaks produced significantly elevated firing rates and the smaller peaks fired at least at 50% of the maximum firing rate. *C*: proportion of units having 1, 2, or >3 excitatory peaks for each MGB subdivision. MGV neurons had the highest proportion of single-peaked units, significantly higher than MGAD or MGPD neurons.

Most MGB neurons (102/134 units) exhibited one excitatory peak in response to pure tones (Fig. 4C). This was especially true for MGV, where 86% of neurons were single peaked (Table 1). Neurons in MGAD (44%) and MGPD (42%) were much more likely to exhibit multipeaked responses (Table 1). Most secondary excitatory peaks (23/32; 72%) were found at frequencies below BF. One-half of the frequency differences (16/32) were found within 0.5 octaves of BF, whereas the others were found at more distant frequencies. There were no obvious preferences for particular frequency differences between BF and second excitatory peaks.

Many MGB neurons (50/134) also exhibited statistically significant inhibition in their frequency tuning curves in addition to excitation (Table 1). Significant inhibition was common in MGV (62%) but was less frequent in MGAD (22%) and MGPD (38%). Of the 50 inhibited neurons, most showed one inhibitory peak (42/50; 84%). Statistically significant inhibition often occurred near BF, such as the examples in Fig. 3, *A*–*D*, and Fig. 4, *A* and *B*. Forty-nine percent of inhibitory peaks (27/55) were within 0.5 octaves of BF and considered as lateral inhibition. In addition, inhibition was also present at frequencies distant from BF such that 51% (28/55) of inhibitory peaks occurred at least 0.5 octaves away from BF. Unlike in auditory cortex (Kadia and Wang 2003), there were no obvious preferences in MGB neurons for particular frequency differences between inhibitory peaks and BF.

Rate-level functions. Once a BF had been identified, the sensitivity of the neuron to sound level was tested by presenting BF tones at different sound levels to produce a firing rate vs. level function. Throughout the MGB in marmosets, most neurons (102/131; 78%) were nonmonotonic in their rate-level functions, often strongly so. Neurons were classified as monotonic, weakly nonmonotonic, or strongly monotonic based on their monotonicity index, which is the ratio of their total firing rate (sum of driven plus spontaneous rates) at the loudest sound level (80 dB SPL for nearly all units) divided by the total firing rate at best level (maximum firing rate). The value of the monotonicity index ranges between 0 and 1. Neurons with a monotonicity index ≥ 0.75 were considered monotonic, those with a monotonicity index between 0.25–0.75 were considered weakly nonmonotonic, and those with indexes <0.25 were considered strongly nonmonotonic. Examples of nonmonotonic rate-level functions are shown in Fig. 5, *A*–*C*. The neuron in Fig. 5*A* had a low threshold, peaked within 20 dB of threshold, and was strongly nonmonotonic. At higher sound levels, the evoked response was completely suppressed for the duration of the sound (Fig. 5*A*, *left*, shaded region). In addition, a strong offset response appeared whose increase in response strength mirrored the decline of the evoked response during the stimulus (Fig. 5*A*, *right*, dashed line). The neuron shown in Fig. 5*B* had a low threshold (0 dB SPL) and was weakly nonmonotonic. Its rate then increased to a maximum rate at 40 dB. In Fig. 5*C*, the response went from threshold to peak within 10 dB, plateaued for 20 dB, and then fell sharply. However, this response was unusual in that the response rebounded at the highest sound levels due to the reappearance of an onset response and a weak sustained response (Fig. 5*C*). The examples in Fig. 5, *A*–*C*, were MGV neurons, but nonmonotonic responses were prevalent in all subdivisions (Table 2 and Fig. 6*A*). Overall, 22% (29/131) of neurons were monotonic. Figure 5*D* provides an example of a neuron that had a monotonic rate-level function and increased its firing rate monotonically in both the onset and sustained portions of the response. The latency of the neuron in Fig. 5*D* decreased with increases in sound level, which was typical of monotonic rate-level responses.

Figure 6*A* plots the distribution of monotonicity index for each MGB subdivision. There were no significant differences in the proportions of monotonic and nonmonotonic units among different MGB subdivisions, although there was a tendency for MGPD neurons to be more monotonic. The classification of units as monotonic, weakly nonmonotonic, or

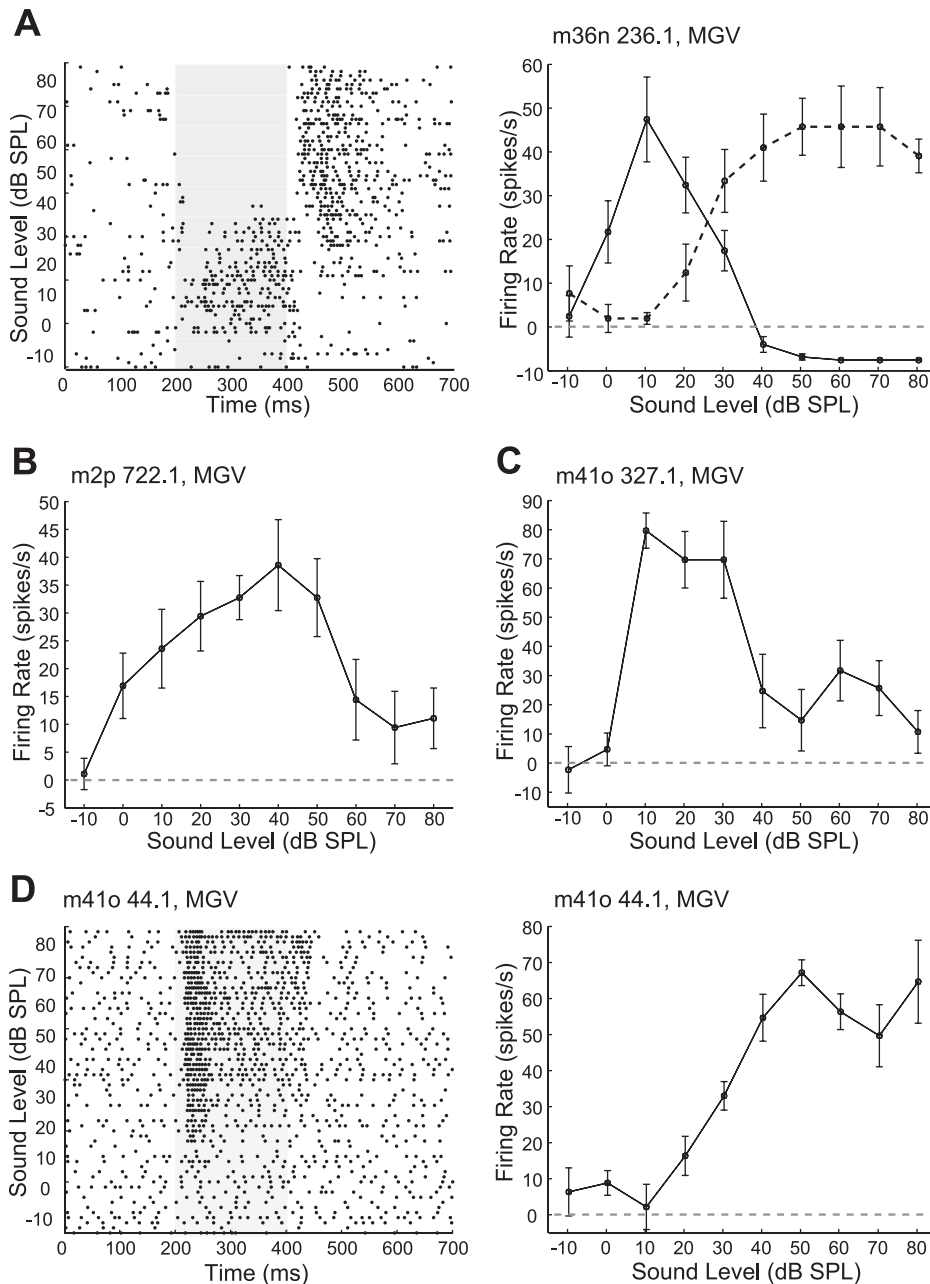


Fig. 5. Neurons with strongly nonmonotonic rate-level functions are common throughout the MGB. In examples shown in A–C, tones were presented at the unit's best frequency and sound level was varied from -10 to 80 dB SPL in 10 -dB steps. All examples are MGV units, but nonmonotonic responses were common in all subdivisions. A, left: dot raster plot of responses of MGV unit m36n-236.1 as tone level is changed. Frequency = 4.92 kHz. A, right: driven firing rate as a function of sound level for MGV unit m36n-236.1. Solid line is firing rate during tone stimulation. Dashed line is offset rate computed from 0 to 200 ms after stimulus offset. B: driven firing rate as a function of sound level for MGV unit m2p-722.1. Frequency = 11.31 kHz. C: driven firing rate as a function of sound level for MGV unit m41o-327.1. Frequency = 9.72 kHz. D, left: dot raster plot of responses of MGV unit m41o-44.1. Frequency = 6.96 kHz. D, right: driven firing rate as a function of sound level for MGV unit m41o-44.1.

strongly nonmonotonic roughly corresponds to three groups that are evident in the distribution of MGB monotonicity index. Further analyses shown in Figs. 6B and 7E and in Table 3 suggest that these three populations differ in other response properties, as well.

Given the presumed differences in the level-dependent balance of excitation and inhibition between monotonic and nonmonotonic neurons, we wanted to investigate whether the shapes of the rate-level functions were similar between populations separated by monotonicity index. Figure 6B compares the normalized responses of strongly nonmonotonic ($n = 46$), weakly nonmonotonic ($n = 56$), and monotonic ($n = 29$) units within a range of ± 30 dB relative to a unit's best level. Note that the total firing rate, rather than the driven rate, was used to match the measurement of monotonicity index, but the results are very similar. Strongly nonmonotonic units were more

sensitive to sound level changes around best level than the other two populations, with firing rates dropping by $\sim 50\%$ as little as ± 10 dB from the best level (Fig. 6B, green line). Strongly nonmonotonic responses were significantly weaker than weakly nonmonotonic and monotonic responses for all sound levels less than best level and for sound levels 10 dB greater than best level (Fig. 6B, yellow circles; $P < 0.05$, Kruskal-Wallis test). For sound levels ≥ 20 dB above best level, monotonic responses were significantly stronger than nonmonotonic and strongly nonmonotonic responses (Fig. 6B, cyan squares; $P < 0.05$, Kruskal-Wallis test). Despite differences in normalized firing rates with respect to level, there were no significant differences among the three populations for spontaneous rate or firing rate at best level (Table 3). However, weakly nonmonotonic units showed significantly broader frequency tuning than strongly nonmonotonic units (Table 3).

Table 2. Rate-level properties by MGB subdivision

	MGV	MGAD	MGPD
Monotonicity index	0.43 ± 0.34 (74)	0.41 ± 0.30 (25)	0.57 ± 0.32 (20)
Nonmonotonic, %	80 (74)	84 (25)	65 (20)
Strongly nonmonotonic, %	39 (74)	36 (25)	20 (20)
Best level, dB SPL	41 ± 23 (74)	44 ± 19 (25)	70 ± 53 (20)
Threshold to best level, dB	14 ± 21 (74)	19 ± 21 (25)	9 ± 20 (20)
RL width, dB	25 ± 15 (59)	28 ± 12 (21)	32 ± 27 (13)
RL dynamic range, dB	34 ± 22 (15)	26 ± 20 (4)	26 ± 23 (7)
RL threshold, dB SPL	27 ± 20 (74)	25 ± 23 (25)	28 ± 23 (20)
RL latency, ms	25.0 ± 20.1 (69)	35.3 ± 43.0 (25)	60.1 ± 59.2 (18)
RL latency median, ms	18.4 (56)	19.6 (25)	28.2 (18)
Latency >50 ms, %	14 ^a	20	44

Values are means ± SD; numbers in parentheses indicate number of units. RL, rate-level. ^aP < 0.05 vs. MGPD, χ^2 test.

There was no correlation between monotonicity index and responses to amplitude-modulated sounds, in terms of either preferred modulation rate or maximum synchronization rate (Table 3).

Best level did not differ between MGB subdivisions (Fig. 7A), but it did differ according to the monotonicity index (Table 3). Weakly nonmonotonic units had significantly lower best levels

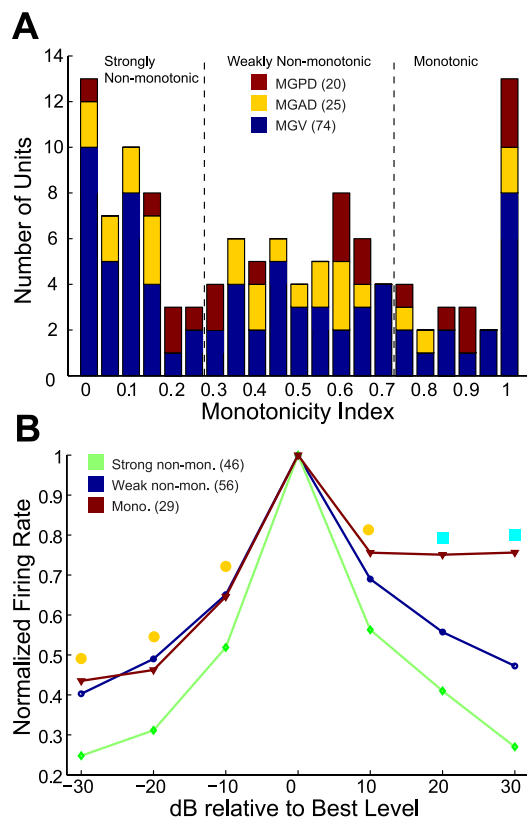


Fig. 6. Population characteristics of MGB rate-level functions. A: distribution of monotonicity index (see METHODS) for MGB units. The number of units producing strongly nonmonotonic (left), weakly nonmonotonic (middle), or monotonic rate-level functions (right) is plotted for each subdivision. Dashed vertical lines segregate monotonic (index > 0.75), weakly nonmonotonic (index 0.25–0.75), and strongly nonmonotonic populations (index < 0.25). B: normalized rate-level functions, with maximum firing rate normalized to 1, for monotonic units (red line), weakly nonmonotonic units (blue line), and strongly nonmonotonic units (green line). Yellow dots indicate that monotonic and weakly nonmonotonic units with monotonicity index > 0.25 (red and blue lines) had significantly higher normalized firing rates than those with ratios < 0.25 (strongly nonmonotonic). Cyan squares indicate that the 3 populations were all significantly different from each other.

Table 3. Rate-level and other tuning properties by monotonicity index

	Weakly Monotonic	Nonmonotonic	Strongly Nonmonotonic
Spontaneous rate, spikes/s	8.7 ± 4.6	8.5 ± 5.6	8.1 ± 6.2
Peak rates, spikes/s	28.7 ± 41.4	24.3 ± 22.2	32.4 ± 25.0
Latency, ms	34.4 ± 35.1 (28)	32.7 ± 41.7 (53)	43.9 ± 52.9 ^a (43)
Median latency, ms	18.7	15.9	23.7
Best level, dB SPL	56 ± 24 ^b	43 ± 23	30 ± 18 ^c
RL threshold, dB SPL	38 ± 24	28 ± 20	20 ± 17 ^d
Level halfwidth, dB	NA	31 ± 20 (50)	22 ± 9 ^e (42)
Frequency halfwidth, octave	0.16 ± 0.14 (18)	0.22 ± 0.18 (40)	0.13 ± 0.10 ^f (35)
AM Fmax, Hz	74 ± 214 (15)	137 ± 274 (30)	128 ± 241 (31)
Nonsynchronized AM, %	17 (18)	21 (38)	6 (33)

Values are means ± SD; numbers in parentheses indicate number of units for which measurements were obtained from a total of 29 monotonic, 56 weakly nonmonotonic, and 46 strongly monotonic units. AM, amplitude modulated; Fmax, maximum modulation frequency at which units are synchronized. ^aP < 0.03 vs. weakly nonmonotonic, Kruskal-Wallis test. ^bP < 0.005 vs. weakly nonmonotonic and strongly nonmonotonic, Kruskal-Wallis test. ^cP < 0.002 vs. weakly nonmonotonic, Kruskal-Wallis test. ^dP < 0.03 vs. weakly nonmonotonic and monotonic, Kruskal-Wallis test. ^eP < 0.05 vs. weakly nonmonotonic, Kruskal-Wallis test. ^fP < 0.01 vs. weakly nonmonotonic, Kruskal-Wallis test.

than monotonic units (Table 3) and significantly higher best levels than strongly nonmonotonic units (Table 3).

To assess the range over which MGB neurons are able to represent sound level in their firing rates, the width of the rate-level curve at half-maximum was measured for nonmonotonic units (Fig. 7B), and the dynamic range (best level minus threshold) was measured for monotonic responses (Fig. 7C). No differences were observed across subdivisions (Fig. 7, B and C), but strongly nonmonotonic units had significantly narrower halfwidths than weakly nonmonotonic units (Fig. 6B and Table 3). Forty-two percent (39/93) of the nonmonotonic MGB neurons were quite sensitive to sound level as indicated by their small dynamic range (≤ 20 dB). Conversely, 27% of monotonic units were sensitive over a broad range of sound levels as indicated by a dynamic range ≥ 50 dB.

To test for the possibility that many neurons classified as nonmonotonic only decreased their firing rates at the highest sound levels, we compared the firing rates 20 dB above the peak level with the peak firing rates. Monotonic units and units whose best levels were ≥ 60 dB were excluded from this analysis. Of the remaining neurons, 20% (17/81) decreased their rates by $< 50\%$, so their rate-level functions were considered plateaued over this range. The other neurons (64/81; 80%) decreased their rates by $> 50\%$, further indicating that many nonmonotonic neurons responded strongly only over a narrow range of sound intensities and responded poorly to sound levels substantially above best level.

Thresholds to tone stimuli. Fifty-six percent (73/131) of the neurons had excitatory thresholds of 20 dB SPL or less (Fig. 2C). There were no significant differences in thresholds between subdivisions (Table 2). However, neurons with strongly nonmonotonic rate-level responses had significantly lower thresholds than those with monotonic or weakly nonmonotonic rate-level responses (Table 3). There was a trend toward more monotonic responses in MGPD, with a higher average monotonicity index and best level, but this did not reach statistical significance.

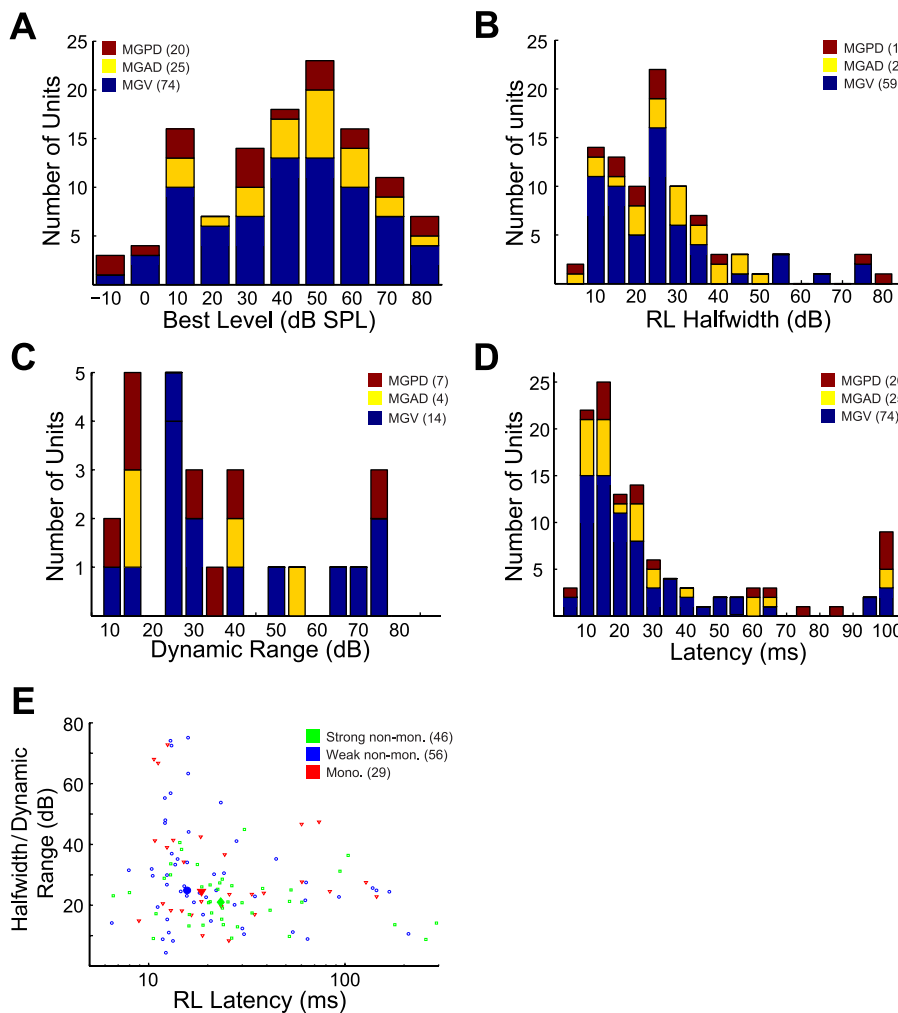


Fig. 7. Sound level tuning in MGB neurons. **A:** histogram of best level for different MGB subdivisions. **B:** histogram of the tuning width at half-maximum rate for the rate-level (RL halfwidth) function of nonmonotonic responses. **C:** histogram of the dynamic range (best level minus threshold level) for the rate-level function of monotonic responses. **D:** histogram of tone response latency. MGV units ($n = 69$, median = 18.4 ms) had a significantly lower proportion of long latency (>50 ms) responses than MGPD units ($n = 20$, median = 38.5 ms) ($P < 0.01$, χ^2 test) but were not significantly different from MGAD units ($n = 25$, median = 15.1 ms). **E:** the level sensitivity, measured as halfwidth for nonmonotonic units and dynamic range for monotonic units, was plotted as a function of tone response latency for monotonic (red triangles), weakly nonmonotonic (blue circles), and strongly nonmonotonic units (green squares). Large symbols indicate median values. Strongly nonmonotonic responses had significantly smaller halfwidths and significantly longer latencies than weakly nonmonotonic responses (Table 3).

Latency-tone stimuli. For each neuron, we also measured the minimum response latency to pure tone stimuli. As shown in Fig. 7D, MGV and MGAD neurons had similar latency distributions. In these subdivisions, most neurons had latencies ≤ 20 ms (51/96 neurons; 53%). Few neurons in MGV (10/71) or MGAD (5/25) had latencies > 50 ms (15/96 total; 16%). The distribution of MGPD latencies was bimodal, with 6/18 neurons having latencies ≤ 15 ms and 8/18 neurons having latencies > 50 ms. The high proportion of long-latency units in MGPD was significantly higher than in MGV (Table 2; $P < 0.05$, χ^2 test). Response latency to tones differed by monotonicity index (Fig. 7E). Strongly nonmonotonic units had significantly longer latencies than weakly nonmonotonic units (Fig. 7E and Table 3). Weakly nonmonotonic and monotonic units had similar latencies.

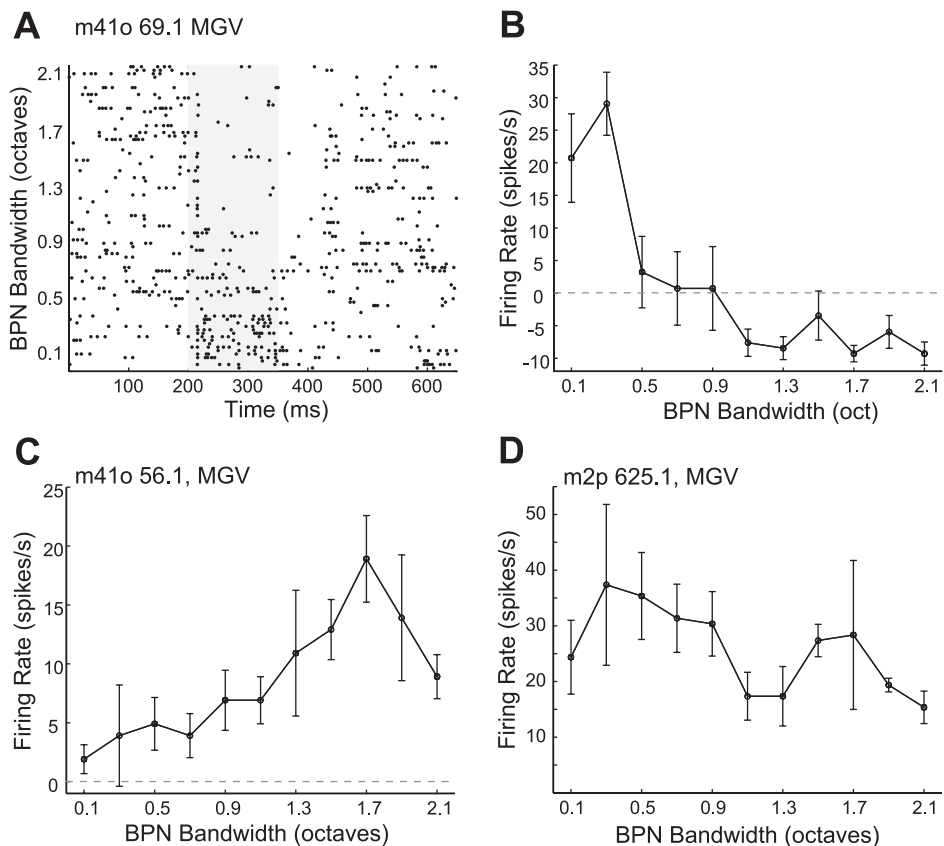
Physiological Properties of MGB Subdivisions: Responses to Noise Stimuli

Noise bandwidth preferences. Another way that we probed the spectral preferences of MGB neurons was by testing their selectivity for the bandwidth of BPN, which has revealed regional differences in primate auditory cortex (Rauschecker and Tian 2004). Examples of preference for noise bandwidth are shown in Fig. 8. Typically, the noise was centered at BF, and the bandwidth was varied from 0.1

to 2.1 octaves in 0.2-octave steps. In Fig. 8, A and B, an MGV neuron responded well only to 0.1- and 0.3-octave stimuli. For bandwidths > 1 octave, the neuron was inhibited. Such a response was common for MGV neurons. Other MGB neurons were not well driven by tone stimuli. These units responded poorly to noises with narrow bandwidths but more strongly to noises with broad bandwidths. In Fig. 8C, an MGV neuron produced small responses for low-bandwidth stimuli. The response strength gradually increased up to a maximum at 1.7 octaves and then decreased. Some neurons exhibited little or no preference for bandwidth under the tested conditions. One example MGV unit shown in Fig. 8D showed strong onset and weak sustained responses over a wide range of bandwidths.

The bandwidth that produced the highest firing rate, referred to as the best bandwidth, was compared across subdivisions in Fig. 9A. We found that MGV neurons had the lowest best bandwidths on average (Fig. 9A and Table 4; median = 0.5 octaves), followed by MGAD neurons (median = 0.5 octaves) and MGPD neurons (median = 0.9 octaves). Furthermore, MGV and MGAD neurons had significantly higher proportions of units whose best bandwidths were ≤ 0.5 octaves (23/44 and 12/23 units, respectively) than MGPD units (6/34 units; $P < 0.05$, χ^2 test). To measure how selective units were for low or high bandwidths, we

Fig. 8. Examples of preference for narrow and broad noise bandwidths. *A*: dot raster plot showing responses of MGV unit m41o-69.1 to bandpass noise (BPN) stimuli of different bandwidths centered on the neuron's BF. In all examples A–C, bandwidth was measured in octaves and was varied from 0.1 to 2.1 octaves in 10 steps. Center frequency = 9.66 kHz. Sound level = 50 dB. *B*: firing rate as a function of noise bandwidth for MGV unit m41o-69.1. *C*: firing rate as a function of noise bandwidth for MGV unit m41o-56.1. Center frequency = 13.5 kHz. Sound level = 50 dB. *D*: firing rate as a function of noise bandwidth for MGV unit m2p-625.1. Center frequency = 2.46 kHz. Sound level = 50 dB. The firing rates shown are for the 100 ms of stimulation, and there was little spiking during the last 100 ms of stimulation for this unit.



also calculated a bandwidth bias for each unit. This was the difference between the maximum firing rate for bandwidths ≤ 0.5 octaves and the maximum firing rate for bandwidths > 1.0 octaves, divided by their sum. Similar results were obtained if we used the average firing rates for these bandwidth ranges. Bandwidth preference ratios less than -0.2 or greater than 0.2 indicate a preference for broadband or narrowband noises, respectively. As shown in Fig. 9*B*, MGV neurons exhibited a preference for narrow bandwidths that was significantly stronger than that of MGPD neurons ($P < 0.05$, Kruskal-Wallis test). There was a trend toward stronger narrowband responses for neurons located more laterally in MGV, but this was not statistically significant. MGAD neurons often did not have any preference for bandwidth, whereas MGPD neurons often preferred broadband rather than narrowband noise stimuli (Fig. 9*B* and Table 4).

Preference to tone or noise stimuli. Figure 9*C* summarizes the tone and noise preferences for each subdivision for all units tested with both tone and noise stimuli, including units that were not driven or were inhibited by at least one of the stimuli. Units in MGV and MGAD were usually significantly excited by both tone and noise stimuli ($P < 0.05$ vs. spontaneous rate, rank-sum test) (55/87 units; 63%). In these subdivisions, it was uncommon for neurons to be responsive only to tones (14/87 units; 16%), only responsive to noise stimuli (11/87 units; 13%), or inhibited by both stimuli (7/87 units; 8%). As a population, MGPD had a unique profile in that it was uncommonly driven by both tone and noise stimuli but was relatively often driven only by noise stimuli or inhibited by both tone and noise stimuli (Fig. 9*C*).

Physiological Properties of MGB Subdivisions: Responses to Temporally Modulated Stimuli

Click response properties. Using either rectangular or Gaussian tone click trains, we found that responses to clicks clearly delineated MGB subdivisions. Some MGB neurons were poorly driven by broadband, rectangular clicks and responded with much higher firing rates when brief tones were shaped by a Gaussian envelope (Bartlett and Wang 2007). The distribution of click response type differed between MGPD and the other two subdivisions (Fig. 10*A* and Table 5). Our earlier study showed that MGB neurons responded to slower temporal modulations (lower click rates in this case) with stimulus-synchronized discharges and faster temporal modulations with nonsynchronized changes in firing rate (Bartlett and Wang 2007). For many neurons with nonsynchronized discharges, there was no increase in firing rate at lower click rates. We also found that some MGB neurons also exhibited synchronized responses at lower click rates and rate representations at higher click rates, which was called the mixed response (Bartlett and Wang 2007). Most neurons in MGV and MGAD showed either synchronized or mixed responses to click train stimuli (Fig. 10*A*). In contrast, most MGPD neurons showed nonsynchronized responses to click train stimuli (17/24 units), a pattern that was not commonly observed for MGV and MGAD subdivisions ($P < 0.05$ vs. MGV, MGAD, χ^2 test). The maximum click frequency at which responses were synchronized (click Fmax) also differed among MGB subdivisions. Figure 10*B* shows the distributions of Fmax for the MGB subdivisions. MGV and MGAD units had the highest Fmax values and were significantly higher than MGPD ($P < 0.05$, Kruskal-Wallis

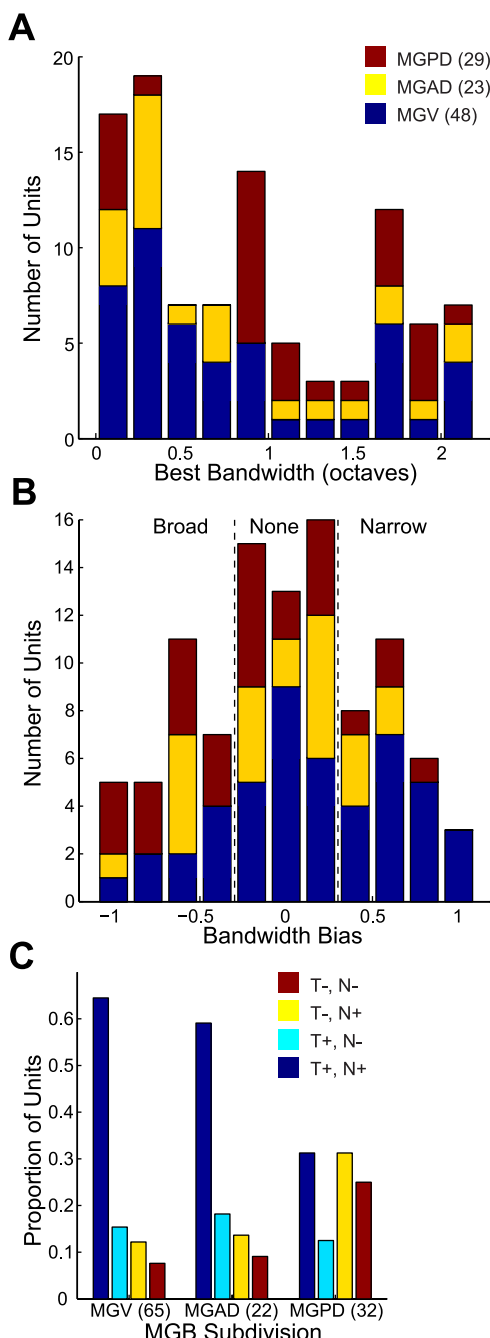


Fig. 9. MGV units prefer narrow bandwidths, whereas other subdivisions exhibit weaker preferences. *A*: normalized histogram of best bandwidth for each MGB subdivision. The best bandwidth was defined as the bandwidth that produced the maximal firing rate. *B*: histogram of units preferring narrow bandwidths vs. broad bandwidths as assessed by the bandwidth bias. Dashed lines separate broad-preferring (Broad; bias less than -0.2), no preference (None; bias between -0.2 and 0.2), and narrow-preferring units (Narrow; bias >0.2). *C*: proportion of units responsive to tones or noise for each subdivision. Blue bars indicate significant excitatory responses to tones and noise (T^+, N^+). Cyan bars indicate significant excitatory responses to tones and nonsignificant or inhibitory responses to noise stimuli (T^+, N^-). Yellow bars indicate significant excitatory responses to noise stimuli and nonsignificant or inhibitory responses to tone stimuli (T^-, N^+). Red bars indicate nonsignificant and inhibitory responses to tones and nonsignificant or inhibitory responses to noise stimuli (T^-, N^-).

test). The latency of the response to click stimuli showed differences among subdivisions (Fig. 10C and Table 5). MGAD units responded on average with the shortest latencies, significantly shorter than all other subdivisions. MGV and MGAD neurons had significantly shorter latencies than those found in MGPD (Fig. 10C; $P < 0.05$, Kruskal-Wallis test). Many MGPD neurons had response latencies >50 ms (10/21 units). MGAD neurons had on average the most temporally precise responses as assessed by the mean vector strength of the responses averaged over all click rates. The mean vector strength was significantly higher in MGAD than in all other subdivisions (Fig. 10C). MGV had higher mean vector strengths than MGPD neurons ($P < 0.03$, Kruskal-Wallis test). There was a clear relationship between mean vector strength and click response latency (Fig. 10C), with the highest vector strengths occurring in units with the shortest latency responses. Nearly all of these units were from MGV or MGAD.

SAM and NAM response properties. Whereas click stimuli are discrete in time, we also studied MGB responses to continuous, sinusoidally amplitude-modulated stimuli across MGB subdivisions using SAM and/or NAM stimuli. These stimuli were temporally modulated at similar frequencies as the click stimuli, but they were expected to generate sustained responses with multiple spikes per cycle rather than the phasic, often binary responses generated in response to click stimuli. For each unit, values were obtained to characterize the synchronization and rate representations of temporal modulation (Table 5). In Fig. 11A, the rate best modulation frequency (rBMF) was plotted as a function of AM Fmax, the maximum modulation frequency at which units are synchronized. This plot succinctly summarizes the rate and temporal representations of AM stimuli in different MGB subdivisions. If a unit was tested with both SAM and NAM stimuli, the maximum Fmax and rBMF values were used. Similar to the click data, MGAD (Fig. 11A, diamonds) and MGV units (Fig. 11A, circles) could synchronize to higher modulation frequencies than MGPD (Fig. 11A, triangles). MGAD and MGV units also had significantly higher temporal best modulation frequencies (tBMF; Table 5), which were the modulation frequencies to which the neurons best synchronized as assessed by vector strength. Surprisingly, MGAD rBMF was significantly higher than in other MGB subdivisions (median rBMF = 62), including MGV (median rBMF = 19). MGV units were more commonly driven with multiple spikes per cycle for modulation frequencies ≤ 32 Hz compared with MGAD neurons, which contributed to higher rates at lower modulation frequencies. There was a trend toward preferring slower modulation frequencies more caudally in MGB, with only 3/57 MGB units with Fmax ≤ 16 Hz found in the rostral one-third of MGB.

There were also subdivision differences in the maximum firing rates produced by AM stimuli. MGPD neurons responded to AM stimuli with significantly lower firing rates than the other subdivisions (modulation frequencies ≤ 128 Hz; Table 5; $P < 0.05$, Kruskal-Wallis test). MGV neurons commonly responded to higher modulation frequencies (>128 Hz) with significantly higher firing rates than the other subdivisions (Table 5). Despite differences in the maximum firing rates, rate-based tuning to modulation frequency was similar across subdivisions, with the halfwidth averaging three to four octaves throughout the auditory thalamus (Table 5).

Table 4. Spectral bandwidth preferences by MGB subdivision

	MGV	MGAD	MGPD
Best BPN bandwidth, octave	0.79 ± 0.65 ^a (40)	0.81 ± 0.70 (22)	1.07 ± 0.63 (28)
Bandwidth preference ratio	0.20 ± 0.79 (40)	-0.04 ± 0.58 (22)	-0.12 ± 0.84 (28)
Narrow preferring, %	55 ^b	50	21
Broad preferring, %	25	36	43
T+, N+, %	65 (49)	59 (22)	31 (32)
T+, N-, %	18 (49)	18 (22)	13 (32)
T-, N+, %	10 (49)	14 (22)	31 (32)
T-, N-, %	7 (49)	9 (22)	25 (32)

Values are means ± SD; numbers in parentheses indicate number of units. BPN, band-pass noise; T+, N+, significant excitatory responses to tones and noise stimuli; T+, N-, significant excitatory responses to tones and nonsignificant or inhibitory responses to noise stimuli; T-, N+, significant excitatory responses to noise stimuli and nonsignificant or inhibitory responses to tone stimuli; T-, N-, nonsignificant and inhibitory responses to tones and nonsignificant or inhibitory responses to noise stimuli. ^a $P < 0.05$ vs. MGPD, Kruskal-Wallis test. ^b $P < 0.05$ vs. MGPD, χ^2 test.

When SAM and NAM Fmax were compared for the same unit, MGV and MGAD values were similar for both SAM and NAM (Fig. 11B). MGPD generated higher Fmax for SAM stimuli due to the prevalent nonsynchronized responses to NAM stimuli (6/11 units). When SAM and NAM firing rates were compared in the same unit, MGV and MGAD units produced higher firing rates for SAM tone stimuli, whereas MGPD neurons produced higher firing rates for NAM stimuli (Fig. 11C).

DISCUSSION

Summary of Results

Using anatomic and physiological criteria, we were able to distinguish three subdivisions in the main portion of the MGB, lateral to the medial and suprageniculate divisions of MGB. Most units in the present study, regardless of MGB subdivision, had narrowly tuned tone responses (when a unit responded to tones) and nonmonotonic rate-level functions. However, each subdivision could be distinguished by a number of features. Figure 12 summarizes the properties of each of the subdivisions as well as showing their relative locations in a schematic of a sagittal MGB section (rostral at right, dorsal at top). MGV was characterized by the strongest parvalbumin staining, weak to moderate calbindin staining, sharp, short-latency, single-peaked tone responses shaped by lateral inhibition, and rapid temporal processing (Fig. 12, MGV). Overall, calbindin labeling increased going from rostral to caudal, whereas parvalbumin labeling was strongest laterally throughout the MGV and MGAD. MGAD neurons were found dorsal to MGV (Fig. 12, MGAD). MGAD neurons were characterized by low-frequency BFs, sharp but often multipeaked tone tuning, and the shortest latency, highest vector strength, highest Fmax, and highest rBMF responses to temporally modulated stimuli. MGPD neurons were found caudal and dorsal relative to MGV. MGPD neurons were different than the other two divisions in a variety of ways (Fig. 12, MGPD). Parvalbumin staining was lower than MGV and calbindin staining was higher compared with the other subdivisions (Fig. 1). MGPD neurons often did not respond to tones or were inhibited by tone and noise stimuli. Many MGPD responses were long latency. Most MGPD neurons had nonsynchronized responses to temporally modulated stimuli.

Subdivisions of Marmoset MGB

The anatomic parcellation of the MGB conforms in large part to that previously described in the marmoset (de la Mothe et al. 2006) and the macaque (Hackett et al. 1998; Molinari et al. 1995). These studies used Nissl, myelin, acetylcholinesterase, cytochrome oxidase, parvalbumin, and calbindin staining to segregate MGB subdivisions and defined separate ventral, anterodorsal, and posterodorsal divisions, which correspond to MGV, MGAD, and MGPD in the present study. In the macaque and in the marmoset, a “transition zone” was described at the conjunction of MGV, MGAD, and MGPD (de la Mothe et al. 2006; Hackett et al. 1998; Molinari et al. 1995). In the marmoset study, it was mentioned that MGV “emerged near the caudal pole” (de la Mothe et al. 2006), which was not observed in our sections, but the sections in that study were cut “perpendicular to the long axis of the brain stem,” rather than in a coronal plane.

A caveat to assigning a recorded unit to a given anatomic subdivision is that units were recorded over a period of months for a given animal and one to three electrolytic lesions were made in physiologically identified regions near the end of recording from an animal. Therefore, the estimate of location is not as precise as if lesions were made over a shorter period of time or for a larger number of tracks. In terms of understanding the correlations of subdivision and location vs. physiological properties in the marmoset MGB, our results suggest that the clearest differences are along the rostrocaudal and dorsoventral dimensions. These dimensions mainly separate the MGAD and MGV, whose physiological properties are consistent with the auditory core pathways, from the MGPD, whose physiological properties are consistent with the auditory belt pathways. MGAD and MGV neurons share many properties, so slight mislocalizations in the dorsoventral dimension that would affect the assignment of a small number of units to MGV or MGAD are unlikely to change the overall population responses of either region. Within MGV and MGAD, neurons with nonsynchronized responses or those preferring slower modulation frequencies were found more caudally. This is similar to the rostrocaudal gradient of temporal modulation preferences in the cat IC (Rodriguez et al. 2010). This suggests that slight mislocalizations in the rostrocaudal dimension that may classify some MGPD units as caudal MGV or MGAD would, if anything, sharpen the differences between MGPD and MGV/MGAD. Along the lateromedial dimension, there were perhaps subtle differences in lateral MGV compared with medial MGV

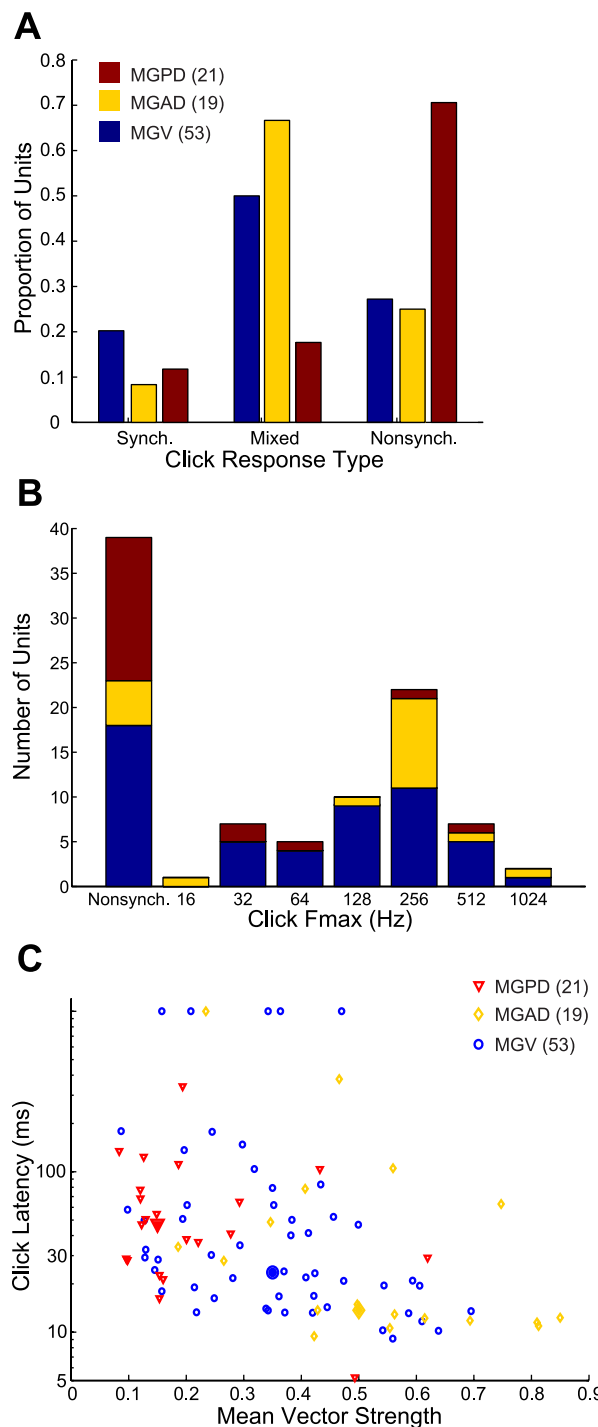


Fig. 10. Click stimuli reveal subdivision differences in temporal processing. *A*: normalized histogram showing the click response type for each subdivision. Response types (synchronized, mixed, nonsynchronized) are defined in METHODS and in Bartlett and Wang (2007). The number of units shown in parentheses in the legend applies to *A*, *B*, and *D*. Sync., synchronized; Nonsynch., nonsynchronized. *B*: histogram showing click Fmax, which is the maximum frequency at which responses are synchronized. Values are means \pm SE. MGV ($n = 53$) and MGAD ($n = 19$) had significantly higher Fmax than MGPD ($n = 21$) ($P < 0.01$, Kruskal-Wallis test). *C*: plot showing relationship between mean vector strength and click response latency. Across MGB subdivisions, lower mean vector strengths were associated with longer latencies, and the highest mean vector strengths were associated with the shortest latencies.

such that lateral MGV neurons were more likely to show preferences for faster modulation frequencies and for tones rather than broadband sounds, but more units would be needed to strengthen that assertion. There were no stark differences between the units recorded more laterally compared with those recorded medially in any subdivision, so slight mislocalizations in the lateromedial dimension that includes a small number of MGM neurons would not substantially alter the average response properties of any subdivision. Unlike studies in the guinea pig (Wallace et al. 2007), we did not find evidence for highly phase-locked responses in medial MGV. Only 3/36 MGB units (2/21 MGV units) whose Fmax was ≥ 250 Hz were localized to the medial one-third of MGV, MGAD, or MGPD.

Tone and Noise Responses

Previous studies in the guinea pig (Anderson et al. 2007; Edeline et al. 1999; He 2001), rat (Bordi and LeDoux 1994; Zhang et al. 2008), cat (Aitkin and Prain 1974; Calford 1983), bat (Wenstrup 1999), and squirrel monkey (Allon et al. 1981) have compared MGV and MGD responses to tone and/or noise stimuli. However, none of these studies made a distinction between anterodorsal and posterodorsal MGD, although the distinctions between the deep dorsal division and the posterodorsal division described by Calford (1983) may be similar. Moreover, only Calford (1983) and Rodrigues-Dagaeff et al. (1989) separated the responses of MGV units into lateral and medial divisions (MG pars ovoidea). In addition, Rouiller and colleagues (Rodrigues-Dagaeff et al. 1989; Rouiller et al. 1990) separated the MGV along the rostrocaudal dimension.

In the present study, MGV neurons had sharper frequency tuning (Fig. 3E) and stronger preferences for tone or narrow-band noise stimuli than MGPD neurons (Fig. 9). This supports results from previous studies (Anderson et al. 2007; Calford 1983; Cetas et al. 2001; Edeline et al. 1999; Zhang et al. 2008). Quantitatively, MGV frequency tuning in the marmoset (median Q value = 11.7) is significantly higher than that derived from the MGV responses to ripple stimuli in cats (mean = 5.8; Miller et al. 2002). Species differences rather than anesthesia may be the critical factor, since frequency tuning in awake guinea pigs was broader than that in either awake marmosets or anesthetized cats (Edeline et al. 1999). The narrow tuning of MGV neurons in marmosets was clearly shaped by inhibition near BF (Fig. 3, *D* and *E*). Whether the inhibition was due to inhibition of neurons in the projection path to MGB neurons or due to direct inhibitory projections to MGB neurons (Bartlett et al. 2000; Peruzzi et al. 1997; Winer et al. 1996) is difficult to distinguish. Recent evidence (Lee and Sherman 2010) suggests that IC inhibitory input originates from different IC regions than excitation. It also remains to be seen whether the lateral inhibition arises due to excitation of inhibitory interneurons in MGV (Winer 1992) or whether it is generated by ascending inhibitory IC inputs (Bartlett and Smith 1999; Peruzzi et al. 1997; Winer et al. 1996). Support for extrinsic sources of inhibition (IC or thalamic reticular nucleus, TRN) to MGB is given by the results of Suga et al. (1997), who found that blocking GABAergic inhibition in MGB broadened tuning curves and altered level tuning in bats, a species that lacks interneurons in the MGB (Winer et al. 1996). For TRN to

Table 5. Temporal processing abilities by MGB subdivision

	MGV	MGAD	MGPD
Click Fmax synchronized, Hz	215 ± 181 (35)	303 ± 219 (14)	145 ± 153 (5)
Click nonsynchronized, %	34 (53)	26 (19)	76 ^a (21)
Click latency, ms	41.9 ± 42.1 (53)	30.6 ± 26.0 (17)	55.9 ± 37.4 ^b (21)
Latency median, ms	23.6 (53)	14.9 (17)	44.1 (21)
Rate boundary, ms	11.6 ± 18.3 (45)	11.9 ± 14.5 (15)	9.3 ± 10.9 (17)
Click mean VS	0.35 ± 0.16 ^c (53)	0.50 ± 0.22 ^d (19)	0.21 ± 0.14 (21)
AM Fmax, Hz	208 ± 171 ^c (68)	297 ± 241 ^c (29)	68 ± 121 (19)
AM tBMF, Hz	53 ± 82 (68)	46 ± 54 (29)	13 ± 11 ^b (19)
Maximum VS	0.68 ± 0.18 ^c (68)	0.65 ± 0.18 ^c (29)	0.58 ± 0.19 (19)
AM mean VS	0.35 ± 0.13 (68)	0.35 ± 0.15 (29)	0.25 ± 0.14 (28)
AM nonsynchronized, %	18 ^f	10 ^f	54
AM rBMF, Hz	43 ± 60 (68)	84 ± 98 (29) ^g	66 ± 98 (28)
Median rBMF, Hz	19	62	32
Maximum rate ≤128 Hz AM, spikes/s	26.8 ± 18.0 (64)	24.0 ± 13.2 (29)	15.9 ± 10.0 ^b (21)
Maximum rate >128 Hz AM, spikes/s	31.0 ± 20.0 ^h (54)	23.6 ± 15.9 (27)	20.1 ± 20.5 (22)
AM halfwidth, octaves	3.4 ± 2.0 (60)	4.2 ± 2.4 (29)	3.4 ± 1.6 (21)

Values are means ± SD; numbers in parentheses indicate number of units. VS, vector strength; tBMF, temporal best modulation frequency; rBMF, rate best modulation frequency. ^a*P* < 0.01 vs. MGAD and MGV, χ^2 test. ^b*P* < 0.05 vs. MGAD and MGV, Kruskal-Wallis test. ^c*P* < 0.001 vs. MGPD, Kruskal-Wallis test. ^d*P* < 0.01 vs. MGV and MGPD, Kruskal-Wallis test. ^e*P* < 0.05 vs. MGPD, Kruskal-Wallis test. ^f*P* < 0.01 vs. MGPD, χ^2 test. ^g*P* < 0.005 vs. MGV, Kruskal-Wallis test. ^h*P* < 0.03 vs. MGAD and MGPD, Kruskal-Wallis test.

affect the frequency tuning at short latencies, the inhibition would need to be tonically activated.

One surprising result was that although MGV neurons had the sharpest frequency tuning, units in MGAD and MGPD still had clearly defined and narrow frequency tuning curves when the units were responsive to tones. This is in contrast to the poor, broadly tuned responses reported on average for dorsal division neurons in previous studies (Calford 1983; He 2001), although narrowly tuned V-shaped tuning was relatively common in the guinea pig dorsal division (Anderson et al. 2007). It should be noted that MGPD units, although sharply tuned, did not respond to tone stimuli with firing rates as high as MGV units (MGPD: 20.3 ± 16.1 spikes/s; MGV: 35.3 ± 28.2 spikes/s; *P* < 0.02, Kruskal-Wallis test). It is possible that the sharp tuning in MGPD is partially explained by thresholding or that the individual tone inputs to MGPD neurons are weaker than those to MGV, which is consistent with weaker individual synaptic inputs and smaller terminals in rat MGD neurons compared with MGV (Bartlett and Smith 2002; Bartlett et al. 2000; Lee and Sherman 2010). Given the prevalence of near-BF inhibition and moderate spontaneous rates for all subdivisions (Figs. 2A and 3E), another potential explanation is that preserving the natural balance of excitation and inhibition in awake animals allowed the expression of lateral inhibition that is not observed in anesthetized animals.

Although all subdivisions exhibited narrow frequency tuning, the prevalence of multipeaked responses in MGAD and MGPD (Fig. 4C) suggests that the excitatory inputs to these subdivisions are distributed over a wider frequency range and are selectively suppressed by inhibition. This is in contrast to the strong tendency toward single-peaked responses in MGV that suggests they receive inputs from a more restricted frequency range (Fig. 4C). Similar results have been reported comparing the MGV, rostral pole, and MGD in the bat (Wenstrup 1999). It remains to be tested whether the multipeaked responses in the marmoset MGAD and MGPD confer combination sensitivity or frequency modulation (FM) selectivity, but it has been shown that in bat MGD, particularly the rostral MGD, neurons are much more likely than MGV neurons to

have such selectivity for complex stimuli (Olsen and Suga 1991; Wenstrup 1999). Unlike the primary auditory cortex, where inhibition often occurred at harmonically related intervals relative to BF (Kadia and Wang 2003), inhibition in the MGB often occurred near BF (Fig. 3F). Harmonic inhibition in auditory cortex therefore appears to be generated mainly intracortically.

Further insight into the spectral integration abilities of MGB neurons came from analysis of their responses to BPN stimuli (Figs. 8 and 9). MGV neurons had the strongest preference for tones and narrowband stimuli, with significantly lower best BPN bandwidths (Fig. 9A) and a high proportion of neurons responding much more strongly to narrowband stimuli (Fig. 9B). The decrease in firing rate with increasing bandwidth was probably due to recruiting lateral inhibition in MGV neurons with increasing bandwidth, which could lead to a suppression of the firing rate (e.g., Fig. 8A). Similar bandwidth preferences have been observed in macaque A1 (Rauschecker and Tian 2004), suggesting that the A1 selectivity could have been inherited from MGV neurons. MGPD neurons exhibit the other end of the bandwidth preference spectrum. Few MGPD neurons have best BPN bandwidths ≤0.5 octaves (Fig. 9A), with almost one-half of them responding much more strongly to BPN bandwidths >1 octave (Fig. 9B), and more than one-half were nonresponsive to tone stimuli (Fig. 9C). In between MGV and MGPD, MGAD neurons responded equally well to tones, narrowband noise stimuli, and broadband noise stimuli (Fig. 9).

Latencies for Tones

MGV and MGAD have very similar latency distributions, with most minimum latencies for tone stimuli falling in the 10- to 20-ms range (Fig. 10C). About one-third of MGPD neurons that responded to tones did so at short latencies (<15 ms), but an equal proportion of MGPD neurons responded at very long latencies (>50 ms; Fig. 10C). A similar dichotomy of mean latencies was seen when comparing the MGV and MGD in the cat (Calford 1983), except that there were relatively fewer short-latency MGPD neurons. The latency disparity between

MGV and MGPD is much greater than the latency disparity between the IC central nucleus and IC dorsal cortex (Liu et al. 2006), which are the main auditory inputs to MGV and MGPD, respectively. This suggests two distinct possibilities to explain the long latency of MGPD responses. One possibility is that early inhibition or slow buildup of IC excitation leads to long-latency MGPD responses, possibly through long-latency

or offset responses (He 2001) that are more prevalent in guinea pig MGD. The other possibility is that MGPD neurons are mainly driven directly by longer latency cortical inputs (He and Hashikawa 1998; He et al. 1997; Polley et al. 2007) or indirectly through the cortical excitation of IC dorsal cortex neurons (Herbert et al. 1991; Winer et al. 1998, 2002).

Sound Level Tuning

Nonmonotonic rate-level functions were the dominant type of response in all MGB subdivisions of the marmoset (Figs. 6–8). Given the low proportion (<5%) of nonmonotonic responses in the IC of awake marmosets (Nelson et al. 2009), it seems likely that generation of nonmonotonic responses originates in the MGB in marmosets. The high proportion of nonmonotonic rate-level functions was also found in the marmoset auditory cortex (Bartlett and Wang 2005; Sadogapan and Wang 2008), suggesting that nonmonotonic cortical responses are at least partially inherited from their MGB inputs. The proportion of nonmonotonic units in MGB is higher than has been reported for the IC (Aitkin 1991; Aitkin et al. 1994; Calford 1983; Edeline et al. 1999; LeBeau et al. 2001; Syka et al. 2000), but only slightly higher in some cases (Aitkin 1991; Palombarini and Caspary 1996; Ryan and Miller 1978). There is significant variability in the proportion of nonmonotonic units between studies. This implies that inhibition within the MGB sculpts the level tuning of MGB neurons beyond that which has been inherited from IC inputs, but there may be significant species and methodological differences that affect the extent of inherited inhibition. The sources of inhibition that produce or enhance nonmonotonic MGB responses remain unclear.

Our data make apparent the differences between monotonic and nonmonotonic responses in the ways in which they represent sound level. For louder sound levels, strongly nonmonotonic responses were distinguished by suppression of their firing rates below spontaneous level. This suggests inhibition by inputs to MGB neurons rather than inherited inhibition from IC neurons, where nonmonotonic suppression rarely drives responses below spontaneous rates (Nelson et al. 2009; Ryan and Miller 1978). This implies that the inhibitory inputs producing strong nonmonotonicity in MGB units have higher thresholds than the excitatory inputs and have monotonic rate-level functions. It also leaves open the possibility that weakly nonmonotonic units, with their lower thresholds and shorter latencies (Table 3), have been inherited from IC inputs. Units with monotonic responses had significantly higher thresholds (~10 dB higher) than those with nonmonotonic responses (Table 3). On average, both monotonic and weakly nonmonotonic units rose to a maximal firing rate over a similar

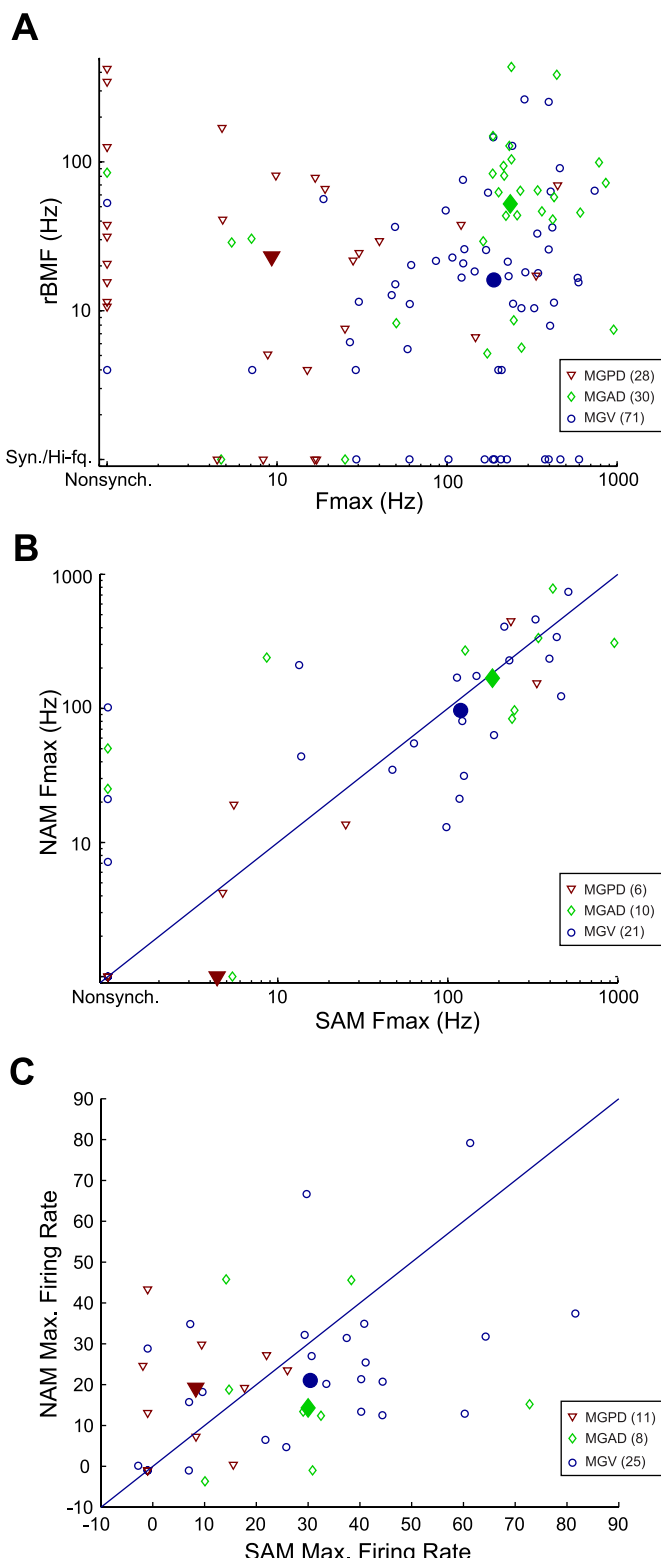


Fig. 11. Amplitude-modulated (AM) stimuli reveal best modulation rates for temporal or rate coding in each subdivision and a comparison of sinusoidally amplitude-modulated tone (SAM) or sinusoidally amplitude-modulated noise (NAM) responses. *A*: rate best modulation frequency (rBMF; weighted by firing rate) plotted as a function of Fmax, or the maximum frequency to which the unit could synchronize. Large filled symbols are median values for each subdivision. Nonsynchronized units were assigned an Fmax value of 1. Units that were synchronized with no significant increases in firing rate or units whose firing rates only increased for modulation frequencies ≥ 256 Hz were assigned an rBMF value of 1. Syn., synchronized; Hi-fq., high frequency. *B*: comparison of SAM and NAM Fmax for individual units. Each unit for which SAM and NAM stimuli were used was plotted. *C*: comparison of SAM and NAM maximum firing rates. Max., maximum.

Fig. 12. Summary of differences and relative locations of MGB subdivisions. Central schematic: schematic sagittal view of marmoset MGB, with dorsal toward the *top* and rostral to the *right*. Colored lines bound the non-MGV subdivisions. MGPD comprises the caudal end of MGB and is found near the dorsal MGB border more rostrally. MGAD comprises the dorsal one-third of the MGB, especially medially and in the central portion of MGB. It forms the rostral tip of MGB and then expands caudally, dorsally, and laterally. The parvalbumin and calbindin profiles along with the differential physiological profiles are given for each subdivision. The medial division and suprageniculate subdivisions, whose physiological properties were not discussed, are not shown. A–D: schematics of convergence patterns from inferior colliculus (IC) to MGB that may generate the spectral, level, and temporal tuning properties observed in MGB neurons. Thalamic reticular nucleus (TRN) inputs are not included in this scheme, although their involvement cannot be ruled out. The shaded IC region in A–D represents a series of cells along a tonotopic gradient, whereas TC represents a single thalamocortical projection neuron. A single interneuron is represented by INT. Green inputs are excitatory, and red inputs are inhibitory. A description of the predicted tuning is shown for each convergence pattern. A: large, ascending IC excitatory and inhibitory inputs with different BFs. B: large, ascending IC excitatory and inhibitory inputs with the same BFs. C: large, ascending IC excitatory inputs to a TC projection neuron and an INT. D: small, ascending IC excitatory and inhibitory inputs with different BFs.

level range, exhibiting an ~35% reduction in firing rates 10 dB below the best level (Fig. 6B). These responses appeared to be separable from strongly nonmonotonic responses. Level tuning in strongly nonmonotonic units was narrow and displayed level responses that sharply declined for deviations from best level of ≤ 10 dB (Fig. 6B, green line). In addition, strongly nonmonotonic units had lower thresholds and longer latencies than weakly nonmonotonic or monotonic units. This suggests that strongly nonmonotonic and weakly nonmonotonic units differ not only in their inhibition above best level but also in their excitation below best level, potentially due to short-latency or tonic inhibition in the IC input to strongly nonmonotonic units. Whether that expression of excitation was inherited from IC inputs or created by differential inhibition remains to be tested.

Nonmonotonic units and monotonic units did not differ significantly in the ranges over which they were able to encode level, as measured by width at half-maximum and dynamic range (threshold to best level), respectively (Fig. 7E). Whereas the MGB dynamic range values for monotonic units were similar to those measured in the marmoset auditory cortex (Wang et al. 2005), the cortical halfwidths were narrower than in the MGB, suggesting that further sharpening of level tuning occurs in auditory cortex. The distribution of the dynamic range of monotonic units was weighted toward either narrow or broad dynamic ranges (Fig. 7C). Wide dynamic range units were found in subdivisions that responded well to tones (Fig. 7C). One possibility is that nonmonotonic units and monotonic units adapt differently in the presence of background noise (Watkins and Barbour 2008).

Temporal Response Properties: Clicks and AM Stimuli

Clicks, SAM tones, and NAM stimuli were used to probe the representation of temporal modulation in MGB neurons in the present study. MGV and MGAD neurons typically represented temporal modulations with stimulus synchronized discharges

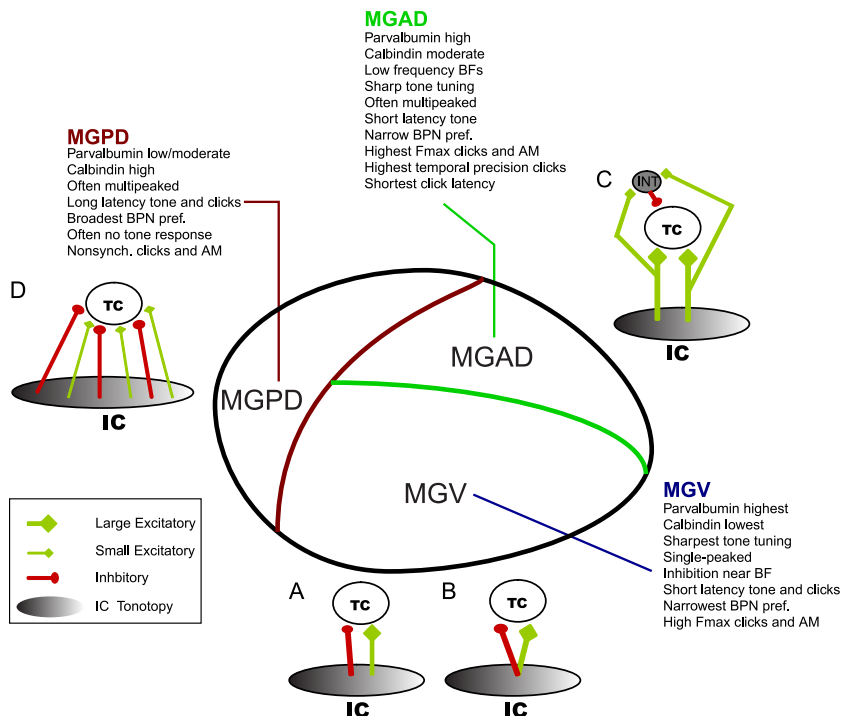


(Fig. 10, A and B), whereas MGPD neurons typically represented temporal modulations with nonsynchronized changes in firing rate. The transformation from synchronized to nonsynchronized representations begins in the auditory thalamus (Bartlett and Wang 2007) and continues in the auditory cortex (Liang et al. 2002; Lu et al. 2001). Previous studies have mainly focused on the stimulus-synchronized discharges in MGV in response to click or SAM stimuli (Creutzfeldt et al. 1980; Miller et al. 2002; Preuss and Muller-Preuss 1990; Vernier and Galambos 1957). Two studies by Rouiller and colleagues (Rouiller and de Ribaupierre 1982; Rouiller et al. 1981) examined responses to click stimuli in different regions of MGB. However, their recordings outside of MGV were mainly from neurons in MGM and SG whose intrinsic properties and connections differ from MGV and MGD neurons (Smith et al. 2006, 2007; Winer 1992). Only seven MGD units were recorded by Rouiller and de Ribaupierre (1982), who reported that MGD units had lower limiting synchronization rates than MGV neurons, but all recorded MGD units were phase-locked. Reasons for not observing nonsynchronized responses in previous studies have been discussed by Bartlett and Wang (2007).

Based on the data in Figs. 10 and 11, the temporal processing properties clearly separate the recorded MGB subdivisions. MGAD potentially seems well-suited for temporal processing of periodicity or for processing sounds with timing cues (e.g., sound localization cues). MGAD units had the highest Fmax, highest mean vector strength, highest rBMFs, and shortest latencies to click stimuli with only MGV neurons having comparably high Fmax values (Figs. 10B and 11A). MGAD units often responded best to low frequencies (Fig. 2B), typically exhibited no preference for narrowband or broadband noise stimuli (Fig. 9B), and had similar Fmax for SAM and NAM stimuli (Fig. 11B), implying that envelope temporal modulations were more important than the carrier. This is

consistent with the idea that MGAD is specialized for temporal processing, with an enhancement of temporal processing and a concomitant lack of sensitivity to the spectral properties of a stimulus. Such a trade-off between spectral and temporal precision has been observed recently in the cat IC (Rodriguez et al. 2010). Finally, MGPD neurons are likely to convert synchronized IC dorsal and external cortex inputs (Muller-Preuss et al. 1994) to nonsynchronized responses, possibly through the integration of many small, facilitating IC synapses (Bartlett and Smith 2002). The long-latency, nonsynchronized MGPD responses to click stimuli (Fig. 10C and Table 5) are consistent with this possibility.

Implications for Auditory Processing Pathways

Auditory-responsive cortical regions have been categorized into “core” and “belt” regions on the basis of their differential connectivities and the relative strengths of their responses to tones vs. band-passed noise stimuli (Kaas and Hackett 2000). For the MGB, classification of subdivisions as core or belt has been based mainly on connectivities with known cortical regions, cytoarchitecture, and chemoarchitecture (de la Mothe et al. 2006; Hackett et al. 1998; Morel et al. 1987) and, to a lesser extent, responsiveness to pure tone stimuli. Whereas studies of MGB response properties in the primate have focused on either spectral properties (Allon et al. 1981) or temporal properties (Preuss and Muller-Preuss 1990), no primate study has attempted to correlate both classes of those properties with location or subdivision within the MGB.

Our results suggest that the marmoset MGPD is very clearly segregated from the other subdivisions in our study in its responses to sound. The auditory response profile of MGPD is consistent with its neuroanatomic classification as being part of the auditory belt and parabelt pathways (Hackett et al. 1998). Despite some similarities in immunostaining and responses to pure tone stimuli, it was also possible to distinguish two other subdivisions of the marmoset MGB, called MGV and MGAD. The differences between subdivisions are summarized in Fig. 12 (central schematic). Based on their short-latency tone responses and moderate to dense parvalbumin staining, these two subdivisions can be categorized as belonging to auditory core pathways. The idea of multiple parallel core pathways was recently demonstrated in the rat thalamocortical pathway (Storace et al. 2010).

What our results imply is that the core region of MGB is not uniform but can be subdivided into at least two subdivisions. These two subdivisions may be specialized for processing different features of sound. MGV neurons have very sharp, single-peaked frequency tuning, good temporal responses, and poor responses to broadband stimuli. As a population, they provide a fine-grained filterbank of the ongoing frequency and intensity content of the sound. The sharpening by lateral inhibition in MGV (Fig. 3) may be analogous to the sharpening of lateral geniculate nucleus (LGN) receptive fields (Solomon et al. 2002; Bonin et al. 2005) to provide a maximum resolution of the sensory map of sound frequency or spatial location. MGAD neurons appear to be suited for temporal processing. MGAD neurons have been shown to project to the caudomedial subdivision (CM) of auditory cortex (de la Mothe et al. 2006), and its response properties are consistent with it providing excitatory input to CM neurons (Kajikawa et al. 2005).

The pathways involving MGAD may function in the dual roles of representing rapid, precise temporal modulations regardless of carrier type, as well as playing a role in sound localization (Tian et al. 2001).

One way that the response profiles to sound stimuli in MGB can be explained is within the framework of a combination of ascending IC excitatory and inhibitory inputs proposed for the rat by Bartlett and Smith (2002) and a slightly modified “driver vs. modulator” scheme developed by Sherman and Guillery (1998). Four schemes are depicted in Fig. 12 that provide testable hypotheses for future studies. In Fig. 12, A and B, MGV frequency tuning results from recruiting a small number of sharply tuned, large-terminal excitatory “driver” IC central nucleus inputs. Lateral inhibition then arises from inhibitory IC inputs whose BFs are either slightly offset from the excitatory BF (Fig. 12A) or with similar BFs that are more broadly tuned than the excitatory inputs. This could create the very sharply tuned, single-peaked responses characteristic of MGV neurons (Figs. 2–4). Given that IC sound level tuning is typically monotonic or weakly nonmonotonic in marmosets and other species, we assume that the strongly nonmonotonic rate-level MGB responses are generated by processing within the MGB. One way that the strong nonmonotonic responses could be generated is by having IC inhibitory inputs that are strong and matched to the BF of the excitatory IC inputs (Fig. 12B), with the IC inhibitory inputs having a monotonic rate-level response. Another way that this could arise would be through the excitation of GABAergic interneurons in MGB by excitatory IC inputs. However, indirect excitation of MGB interneurons would be expected to produce longer latency inhibition after the excitation, which does not fit as well with the complete suppression of responses and longer latencies observed in strongly nonmonotonic responses (Fig. 5A and Table 3). Interneurons are more likely to shape and shorten the duration of the excitatory MGB response. Interneuron inhibition that occurs just after IC excitation could maintain the ability of MGAD and MGV neurons to phase-lock to high modulation frequencies and to increase the temporal precision of MGB responses while maintaining short-latency responses (Fig. 12C). By contrast, MGPD responses would result from recruiting numerous small-terminal, IC dorsal cortex excitatory and inhibitory inputs (Aitkin et al. 1994; Peruzzi et al. 1997) that potentially span a wider frequency range (Fig. 12D). Activation of a small number of these inputs by a tone can produce a small change in firing rates, but activation of many small inputs by a broadband noise could produce a much stronger response in MGPD neurons (Figs. 3 and 9C). Although each of the four proposed connection patterns may be more strongly associated with one subdivision, we do not mean to imply that they are exclusive to any single subdivision.

Further work should transform our understanding of central auditory pathways from a very coarse core vs. belt and tone vs. noise categorization of auditory regions to a fine-grained understanding of the many functional central auditory pathways involved in extracting relevant sound features.

ACKNOWLEDGMENTS

We thank A. Pistorio for excellent assistance in animal maintenance and neuroanatomy; S. Hendry for generous use of facilities, materials, and expertise; and D. Bendor and E. Issa for helpful comments on a draft of the manuscript.

GRANTS

This work was supported by Deafness-Research Foundation Grant BAE.HOPK-03-1C and National Institute on Deafness and Other Communication Disorders Grants DC-06357 to E. Bartlett and DC-03180 to X. Wang.

DISCLOSURES

No conflicts of interest, financial or otherwise, are declared by the author(s).

REFERENCES

- Aitkin L.** Rate-level functions of neurons in the inferior colliculus of cats measured with the use of free-field sound stimuli. *J Neurophysiol* 65: 383–392, 1991.
- Aitkin LM, Prain SM.** Medial geniculate body: unit responses in the awake cat. *J Neurophysiol* 37: 512–521, 1974.
- Aitkin LM, Kudo M, Irvine DR.** Connections of the primary auditory cortex in the common marmoset, *Callithrix jacchus jacchus*. *J Comp Neurol* 269: 235–248, 1988.
- Aitkin LM, Merzenich MM, Irvine DR, Clarey JC, Nelson JE.** Frequency representation in auditory cortex of the common marmoset (*Callithrix jacchus jacchus*). *J Comp Neurol* 252: 175–185, 1986.
- Aitkin L, Tran L, Syka J.** The responses of neurons in subdivisions of the inferior colliculus of cats to tonal, noise and vocal stimuli. *Exp Brain Res* 98: 53–64, 1994.
- Allon N, Yeshurun Y, Wollberg Z.** Responses of single cells in the medial geniculate body of awake squirrel monkeys. *Exp Brain Res* 41: 222–232, 1981.
- Anderson LA, Wallace MN, Palmer AR.** Identification of subdivisions in the medial geniculate body of the guinea pig. *Hear Res* 228: 156–167, 2007.
- Bartlett EL, Smith PH.** Anatomic, intrinsic, and synaptic properties of dorsal and ventral division neurons in rat medial geniculate body. *J Neurophysiol* 81: 1999–2016, 1999.
- Bartlett EL, Smith PH.** Effects of paired-pulse and repetitive stimulation on neurons in the rat medial geniculate body. *Neuroscience* 113: 957–974, 2002.
- Bartlett EL, Wang X.** Long-lasting modulation by stimulus context in primate auditory cortex. *J Neurophysiol* 94: 83–104, 2005.
- Bartlett EL, Wang X.** Neural representations of temporally modulated signals in the auditory thalamus of awake primates. *J Neurophysiol* 97: 1005–1017, 2007.
- Bartlett EL, Stark JM, Guillory RW, Smith PH.** Comparison of the fine structure of cortical and collicular terminals in the rat medial geniculate body. *Neuroscience* 100: 811–828, 2000.
- Bendor D, Wang X.** Neural response properties of primary, rostral, and rostrotemporal core fields in the auditory cortex of marmoset monkeys. *J Neurophysiol* 100: 888–906, 2008.
- Bonin V, Mante V, Carandini M.** The suppressive field of neurons in lateral geniculate nucleus. *J Neurosci* 25: 10844–10856, 2005.
- Bordi F, LeDoux JE.** Response properties of single units in areas of rat auditory thalamus that project to the amygdala. I. Acoustic discharge patterns and frequency receptive fields. *Exp Brain Res* 98: 261–274, 1994.
- Brugge JF, Merzenich MM.** Responses of neurons in auditory cortex of the macaque monkey to monaural and binaural stimulation. *J Neurophysiol* 36: 1138–1158, 1973.
- Calford MB.** The parcellation of the medial geniculate body of the cat defined by the auditory response properties of single units. *J Neurosci* 3: 2350–2364, 1983.
- Calford MB, Aitkin LM.** Ascending projections to the medial geniculate body of the cat: evidence for multiple, parallel auditory pathways through thalamus. *J Neurosci* 3: 2365–2380, 1983.
- Cetas JS, Price RO, Velenovsky DS, Sinex DG, McMullen NT.** Frequency organization and cellular lamination in the medial geniculate body of the rabbit. *Hear Res* 155: 113–123, 2001.
- Creutzfeldt O, Hellweg FC, Schreiner C.** Thalamocortical transformation of responses to complex auditory stimuli. *Exp Brain Res* 39: 87–104, 1980.
- Cruikshank SJ, Killackey HP, Metherate R.** Parvalbumin and calbindin are differentially distributed within primary and secondary subregions of the mouse auditory forebrain. *Neuroscience* 105: 553–569, 2001.
- de la Mothe LA, Blumell S, Kajikawa Y, Hackett TA.** Thalamic connections of the auditory cortex in marmoset monkeys: core and medial belt regions. *J Comp Neurol* 496: 72–96, 2006.
- de Venecia RK, Smelser CB, Lossman SD, McMullen NT.** Complementary expression of parvalbumin and calbindin D-28k delineates subdivisions of the rabbit medial geniculate body. *J Comp Neurol* 359: 595–612, 1995.
- Edeline JM, Manunta Y, Nodal FR, Bajo VM.** Do auditory responses recorded from awake animals reflect the anatomical parcellation of the auditory thalamus? *Hear Res* 131: 135–152, 1999.
- Evans EF.** The frequency response and other properties of single fibres in the guinea-pig cochlear nerve. *J Physiol* 226: 263–287, 1972.
- Hackett TA, Stepniewska I, Kaas JH.** Thalamocortical connections of the parabelt auditory cortex in macaque monkeys. *J Comp Neurol* 400: 271–286, 1998.
- Hashikawa T, Rausell E, Molinari M, Jones EG.** Parvalbumin- and calbindin-containing neurons in the monkey medial geniculate complex: differential distribution and cortical layer specific projections. *Brain Res* 544: 335–341, 1991.
- Hashikawa T, Molinari M, Rausell E, Jones EG.** Patchy and laminar terminations of medial geniculate axons in monkey auditory cortex. *J Comp Neurol* 362: 195–208, 1995.
- He JF.** ON and OFF pathways segregated at the auditory thalamus of the guinea pig. *J Neurosci* 21: 8672–8679, 2001.
- He JF, Hashikawa T.** Connections of the dorsal zone of cat auditory cortex. *J Comp Neurol* 400: 334–348, 1998.
- He JF, Hashikawa T, Ojima H, Kinouchi Y.** Temporal integration and duration tuning in the dorsal zone of cat auditory cortex. *J Neurosci* 17: 2615–2625, 1997.
- Herbert H, Aschoff A, Ostwald J.** Topography of projections from the auditory cortex to the inferior colliculus in the rat. *J Comp Neurol* 304: 103–122, 1991.
- Hu B.** Functional organization of lemniscal and nonlemniscal auditory thalamus. *Exp Brain Res* 153: 543–549, 2003.
- Jones EG.** Chemically defined parallel pathways in the monkey auditory system. *Ann NY Acad Sci* 999: 218–233, 2003.
- Jones EG, Hendry SH.** Differential calcium binding protein immunoreactivity distinguishes classes of relay neurons in monkey thalamic nuclei. *Eur J Neurosci* 1: 222–246, 1989.
- Jones EG, Dell'Anna ME, Molinari M, Rausell E, Hashikawa T.** Subdivisions of macaque monkey auditory cortex revealed by calcium-binding protein immunoreactivity. *J Comp Neurol* 362: 153–170, 1995.
- Kaas JH, Hackett TA.** Subdivisions of auditory cortex and processing streams in primates. *Proc Natl Acad Sci USA* 97: 11793–11799, 2000.
- Kadia SC, Wang X.** Spectral integration in A1 of awake primates: neurons with single- and multipeaked tuning characteristics. *J Neurophysiol* 89: 1603–1622, 2003.
- Kajikawa Y, de La Mothe L, Blumell S, Hackett TA.** A comparison of neuron response properties in areas A1 and CM of the marmoset monkey auditory cortex: tones and broadband noise. *J Neurophysiol* 93: 22–34, 2005.
- LeBeau FE, Malmierca MS, Rees A.** Iontophoresis *in vivo* demonstrates a key role for GABA_A and glycinergic inhibition in shaping frequency response areas in the inferior colliculus of guinea pig. *J Neurosci* 21: 7303–7312, 2001.
- Lee CC, Sherman SM.** Topography and physiology of ascending streams in the auditory tectothalamic pathway. *Proc Natl Acad Sci USA* 107: 372–377, 2010.
- Liang L, Lu T, Wang X.** Neural representations of sinusoidal amplitude and frequency modulations in the primary auditory cortex of awake primates. *J Neurophysiol* 87: 2237–2261, 2002.
- Liu LF, Palmer AR, Wallace MN.** Phase-locked responses to pure tones in the inferior colliculus. *J Neurophysiol* 95: 1926–1935, 2006.
- Lu T, Liang L, Wang X.** Temporal and rate representations of time-varying signals in the auditory cortex of awake primates. *Nat Neurosci* 4: 1131–1138, 2001.
- Miller LM, Escabí MA, Read HL, Schreiner CE.** Spectrotemporal receptive fields in the lemniscal auditory thalamus and cortex. *J Neurophysiol* 87: 516–527, 2002.
- Molinari M, Dell'Anna ME, Rausell E, Leggio MG, Hashikawa T, Jones EG.** Auditory thalamocortical pathways defined in monkeys by calcium-binding protein immunoreactivity. *J Comp Neurol* 362: 171–194, 1995.
- Morel A, Kaas JH.** Subdivisions and connections of auditory cortex in owl monkeys. *J Comp Neurol* 318: 27–63, 1992.
- Morel A, Rouiller E, de Ribaupierre Y, de Ribaupierre F.** Tonotopic organization in the medial geniculate body (MGB) of lightly anesthetized cats. *Exp Brain Res* 69: 24–42, 1987.

- Müller-Preuss P, Flachskamm C, Bieser A.** Neural encoding of amplitude modulation within the auditory midbrain of squirrel monkeys. *Hear Res* 80: 197–208, 1994.
- Nelson PC, Smith ZM, Young E.** Wide-dynamic-range forward suppression in marmoset inferior colliculus neurons is generated centrally and accounts for perceptual masking. *J Neurosci* 29: 2553–2562, 2009.
- Olsen JF, Suga N.** Combination-sensitive neurons in the medial geniculate body of the mustached bat: encoding of relative velocity information. *J Neurophysiol* 65: 1254–1274, 1991.
- Palombi PS, Caspary DM.** Physiology of the aged Fischer 344 rat inferior colliculus: responses to contralateral monaural stimuli. *J Neurophysiol* 76: 3114–3125, 1996.
- Peruzzi D, Bartlett E, Smith PH, Oliver DL.** A monosynaptic GABAergic input from the inferior colliculus to the medial geniculate body in the rat. *J Neurosci* 17: 3766–3777, 1997.
- Pickles JO.** Psychophysical frequency resolution in the cat as determined by simultaneous masking and its relation to auditory-nerve resolution. *J Acoust Soc Am* 66: 1725–1732, 1979.
- Pistorio AL, Hendry SH, Wang X.** A modified technique for high-resolution staining of myelin. *J Neurosci Methods* 153: 135–146, 2006.
- Polley DB, Read HL, Storace DA, Merzenich MM.** Multiparametric auditory receptive field organization across five cortical fields in the albino rat. *J Neurophysiol* 97: 3621–3638, 2007.
- Preuss A, Müller-Preuss P.** Processing of amplitude modulated sounds in the medial geniculate body of squirrel monkeys. *Exp Brain Res* 79: 207–211, 1990.
- Ramachandran R, Davis KA, May BJ.** Single-unit responses in the inferior colliculus of decerebrate cats. I. Classification based on frequency response maps. *J Neurophysiol* 82: 152–163, 1999.
- Rauschecker JP, Tian B.** Processing of band-passed noise in the lateral auditory belt cortex of the rhesus monkey. *J Neurophysiol* 91: 2578–2589, 2004.
- Read HL, Nauen DW, Escabí MA, Miller LM, Schreiner CE, Winer JA.** Distinct core thalamocortical pathways to central and dorsal primary auditory cortex. *Hear Res* 274: 95–104, 2010.
- Rodrigues-Dagaeff C, Simm G, de Ribaupierre Y, Villa A, de Ribaupierre F, Rouiller EM.** Functional organization of the ventral division of the medial geniculate body of the cat: evidence for a rostro-caudal gradient of response properties and cortical projections. *Hear Res* 39: 103–125, 1989.
- Rodríguez FA, Read HL, Escabí MA.** Spectral and temporal modulation tradeoff in the inferior colliculus. *J Neurophysiol* 103: 887–903, 2010.
- Rouiller E, de Ribaupierre F.** Neurons sensitive to narrow ranges of repetitive acoustic transients in the medial geniculate body of the cat. *Exp Brain Res* 48: 323–326, 1982.
- Rouiller EM, Rodrigues-Dagaeff C, Simm G, de Ribaupierre Y, Villa A, de Ribaupierre F.** Functional organization of the medial division of the medial geniculate body of the cat: tonotopic organization, spatial distribution of response properties and cortical connections. *Hear Res* 39: 127–142, 1989.
- Rouiller EM, Capt M, Hornung JP, Streit P.** Correlation between regional changes in the distributions of GABA-containing neurons and unit response properties in the medial geniculate body of the cat. *Hear Res* 49: 249–258, 1990.
- Rouiller E, de Ribaupierre Y, Toros-Morel A, de Ribaupierre F.** Neural coding of repetitive clicks in the medial geniculate body of cat. *Hear Res* 5: 81–100, 1981.
- Rubio-Garrido P, Pérez-de-Manzo F, Clascá F.** Calcium-binding proteins as markers of layer-I projecting vs deep layer projecting thalamocortical neurons: a double labeling analysis in the rat. *Neuroscience* 149: 242–250, 2007.
- Ryan A, Miller J.** Single unit responses in the inferior colliculus of the awake and performing rhesus monkey. *Exp Brain Res* 32: 389–407, 1978.
- Sadagopan SS, Wang X.** Level invariant representation of sounds by populations of neurons in primary auditory cortex. *J Neurosci* 28: 3415–3426, 2008.
- Seiden HR.** *Auditory Acuity of the Marmoset Monkey (Hapale jacchus)*(PhD dissertation). Princeton, NJ: Princeton University, 1957.
- Sherman SM, Guillory RW.** On the actions that one nerve cell can have on another: distinguishing “drivers” from “modulators”. *Proc Natl Acad Sci USA* 95: 7121–7126, 1998.
- Smith PH, Bartlett EL, Kowalkowski A.** Unique combination of anatomy and physiology in cells of the rat paralaminar thalamic nuclei adjacent to the medial geniculate body. *J Comp Neurol* 496: 314–334, 2006.
- Smith PH, Bartlett EL, Kowalkowski A.** Cortical and collicular inputs to cells in the rat paralaminar thalamic nuclei adjacent to the medial geniculate body. *J Neurophysiol* 98: 681–695, 2007.
- Solomon SG, White AJ, Martin PR.** Extraclassical receptive field properties of parvocellular, magnocellular, and koniocellular cells in the primate lateral geniculate nucleus. *J Neurosci* 22: 338–349, 2002.
- Storace FA, Higgins NC, Read HL.** Thalamic label patterns suggest primary and ventral auditory fields are distinct core regions. *J Comp Neurol* 518: 1630–1646, 2010.
- Suga N, Zhang Y, Yan J.** Sharpening of frequency tuning by inhibition in the thalamic auditory nucleus of the mustached bat. *J Neurophysiol* 77: 2098–2114, 1997.
- Syka J, Popelá J, Kvásnák E, Astl J.** Response properties of neurons in the central nucleus and external and dorsal cortices of the inferior colliculus in guinea pig. *Exp Brain Res* 133: 254–266, 2000.
- Tian B, Reser D, Durham A, Kustov A, Rauschecker JP.** Functional specialization in rhesus monkey auditory cortex. *Science* 292: 290–293, 2001.
- Tokuno H, Tanaka I, Umitsu Y, Nakamura Y.** Stereo Navi 2.0: software for stereotaxic surgery of the common marmoset (*Callithrix jacchus*). *Neurosci Res* 65: 312–315, 2009.
- Vernier VG, Galambos R.** Response of single medial geniculate units to repetitive click stimuli. *Am J Physiol* 188: 233–237, 1957.
- Wallace MN, Anderson LA, Palmer AR.** Phase-locked responses to pure tones in the auditory thalamus. *J Neurophysiol* 98: 1941–1952, 2007.
- Wang X.** Neural coding strategies in auditory cortex. *Hear Res* 229: 81–93, 2007.
- Wang X, Lu T, Liang L, Snider RK.** Representations of sound intensity in auditory cortex of awake monkeys. *Soc Neurosci Abst* 35: 282.81–9, 2005.
- Watkins PV, Barbour DL.** Specialized neuronal adaptation for preserving input sensitivity. *Nat Neurosci* 11: 1259–1261, 2008.
- Wenstrup JJ.** Frequency organization and responses to complex sounds in the medial geniculate body of the mustached bat. *J Neurophysiol* 82: 2528–2544, 1999.
- Winer JA.** Identification and structure of neurons in the medial geniculate body projecting to primary auditory cortex (AI) in the cat. *Neuroscience* 13: 395–413, 1984.
- Winer JA.** (editor) *The Functional Architecture of the Medial Geniculate Body and the Primary Auditory Cortex*. Springer Handbook of Auditory Research. New York: Springer, 1992.
- Winer JA, Chernock ML, Larue DT, Cheung SW.** Descending projections to the inferior colliculus from the posterior thalamus and the auditory cortex in rat, cat, and monkey. *Hear Res* 168: 181–195, 2002.
- Winer JA, Larue DT, Diehl JJ, Hefti BJ.** Auditory cortical projections to the cat inferior colliculus. *J Comp Neurol* 400: 147–174, 1998.
- Winer JA, Miller LM, Lee CC, Schreiner CE.** Auditory thalamocortical transformation: structure and function. *Trends Neurosci* 28: 255–263, 2005.
- Winer JA, Saint Marie RL, Larue DT, Oliver DL.** GABAergic feedforward projections from the inferior colliculus to the medial geniculate body. *Proc Natl Acad Sci USA* 93: 8005–8010, 1996.
- Zhang Z, Yu YQ, Liu CH, Chan YS, He J.** Reprint of “Frequency tuning and firing pattern properties of auditory thalamic neurons: an in vivo intracellular recording from the guinea pig.” *Neuroscience* 154: 272–282, 2008.